JOURNAL OF PETROLOGY | VOLUME 41 | NUMBER 7 | PAGES 1127–1153 | 2000

Geochemical Study of Ultramafic Volcanic and Plutonic Rocks from Gorgona Island, Colombia: the Plumbing System of an Oceanic Plateau

S. RÉVILLON*, N. T. ARNDT†, C. CHAUVEL† AND E. HALLOT

GÉOSCIENCES RENNES, CNRS UPR 4661, UNIVERSITÉ DE RENNES 1, CAMPUS DE BEAULIEU, 35042 RENNES CEDEX, FRANCE

RECEIVED SEPTEMBER 17, 1999; REVISED TYPESCRIPT ACCEPTED FEBRUARY 23, 2000

The only known post-Archaean komatiites are found on Gorgona, a small island off the Colombian coast that forms part of the Caribbean oceanic plateau. Mafic and ultramafic intrusions are located in the interior of the island. To establish the relationship between intrusive and extrusive phases of ultramafic magmatism, and to help understand how an oceanic plateau is constructed, we undertook the first petrological and geochemical study of the intrusive rocks. Rare earth element patterns in gabbros range from almost flat to moderately depleted; in dunites and wehrlites, the depletion is more pronounced. These patterns fall midway in the range measured in Gorgona volcanics, whose compositions vary from slightly enriched to extremely depleted. Nd isotope compositions indicate two distinct mantle sources, one highly depleted, the other less depleted. MgO contents of parental liquids are estimated from olivine compositions at 20–25% in ultramafic lavas, and 12–13% in the intrusives. Petrographic observations and similarities in trace-element contents indicate that the two magma types are comagmatic, related through olivine fractionation. Modelling of major and trace elements indicates that the primary ultramafic magmas formed by advanced critical melting at high pressure in a rising mantle plume. The plumbing system that fed the Gorgona plateau was complex, being characterized by a series of magma chambers at different crustal levels. Mantle-derived ultramafic liquids either travelled directly to the surface to erupt as komatiite flows, or were trapped in magma chambers where they differentiated into basaltic liquid and mafic to ultramafic cumulates. Gorgona gabbros and peridotites formed in shallow-level examples of these intrusions.

KEY WORDS: *Gorgona Island, Colombia; komatiite; mantle melting; oceanic plateau; melt transport*

*Corresponding author. Present address: University of Leicester, Department of Geology, University Road, Leicester LE1 7RH, UK. Telephone: +44-116-252-36-29. Fax: +44-116-252-39-18. e-mail: sr58@le.ac.uk

†Present address: LGCA, Université Joseph Fourier, 1381 rue de la Piscine, 38400 Grenoble, France.

INTRODUCTION

Surprisingly little is known about the internal structure and magmatic evolution of oceanic plateaux. This is due in part to the relative inaccessibility of type examples such as Ontong Java and other plateaux in the Pacific, which are located far from continents, in deep waters, and often beneath a deep layer of sediments. Samples obtained by dredging or drilling the submerged portions, or through field work on the few sections exposed on islands around the Ontong Java plateau consist predominantly of tholeiitic basalt with relatively uniform, magmatically evolved compositions (Mahoney *et al.*, 1993; Neal *et al.*, 1997). These compositions are far removed from those of the primary picritic magmas that formed through partial melting of the mantle source at sub-lithosphere depths (Cox, 1980). The generation of basalt from picrite involves crystallization of large volumes of olivine, which presumably accumulated in magma chambers at deeper levels in the plateau. It is commonly assumed that these chambers are located at the base of the crust where magma would pool as it passes from dense mantle peridotite to less dense basaltic rocks. This assumption is supported by geophysical data—layers with high seismic velocities in the lower parts of oceanic plateaux are commonly equated with olivine-rich cumulates (Coffin & Eldholm, 1994; Leroy & Mauffret, 1996; Mauffret & Leroy, 1997)—and from numerical modelling. Farnetani *et al.* (1996) have shown that the seismic structure of oceanic plateaux can be reproduced

in a model of partial melting in a mantle plume and fractional crystallization in a deep-seated magma chamber.

None the less, we have little direct information about the path taken by magma on its way to the surface, nor about the size and location of the magma chambers. In an attempt to obtain such information we undertook a study of intrusive mafic and ultramafic rocks that are exposed in the interior of Gorgona Island, which is located off the coast of Colombia and is believed to be part of the Caribbean oceanic plateau. Preliminary studies by Echeverria (1980) and Kerr *et al.* (1997*a*, 1997*b*, 1998) had shown that the chemical compositions of these intrusive rocks suggested that they were magmatically linked to the mafic to ultramafic lavas preserved on Gorgona Island. It was therefore thought that these intrusions could be the relicts of deep-seated magma chambers within which magma evolved from picrite to basalts. However, the new petrological, geochemical and isotopic data presented in this paper show that the intrusive rocks from Gorgona Island were emplaced at a relatively high level in the plateau and that they were fed by magmas that had already acquired a basaltic composition. Although our study provides only indirect information about the nature of the deeper chamber, it does reveal the complexity of the plumbing system of an oceanic plateau. Rather than involving a single large chamber at Moho depths, an oceanic plateau contains a series of chambers at different depths, some fed by near-primary picritic to komatiitic liquids, others by magma that had evolved to basalt in deeper staging chambers.

GEOLOGICAL BACKGROUND

Caribbean oceanic plateau

The Caribbean oceanic plateau covers most of the floor of the Caribbean basin as well as parts of the South and Central America Pacific coast. Its total area is about 6×10^5 km^2 (Coffin & Eldholm, 1993). The crust of the Caribbean basin has a composite seismic structure and varies in thickness from 5 to >20 km, mostly well in excess of that of 'normal' oceanic crust (Leroy, 1995; Leroy & Mauffret, 1996; Mauffret & Leroy, 1997). Most geologists and geophysicists accept that the plateau formed through partial melting within a mantle plume (Duncan & Hargraves, 1984). Published radiometric ages indicate two or three magmatic events: the first from 90 to 88 Ma, the second at ~76 Ma (Kerr *et al.*, 1997*a*, 1997*b*; Sinton *et al.*, 1998) and a possible third event at ~55 Ma (Révillon *et al.*, 2000). The volume of magma formed during the first event appears to have been larger than for the latter two events, and its formation is linked to melting in the head of a large starting plume. This part of the plateau is thought to have formed 90–88 my ago in the Pacific, and may be linked to the currently active Galapagos hotspot (Duncan & Hargraves, 1984; Pindell *et al.*, 1988; Pindell & Barrett, 1990). The nature of the two younger events is a matter of debate (Hauff *et al.*, 1997; Kerr *et al.*, 1997*a*; Lapierre *et al.*, 2000; Révillon *et al.*, 2000). The northern part of the plateau was transported between the North and South American plates through eastward movement of the Farallon plate, whereas the southern part was accreted along the South and Central America Pacific coast (Burke, 1988; Cloos, 1993; Saunders *et al.*, 1996).

Exposed parts of the Caribbean plateau are composed mainly of basaltic lava flows, with the exception of several series of high-MgO lavas—the komatiites of Gorgona Island, and picrites in many parts of the province (e.g. Curaçao, Colombia, Costa Rica). Plutonic complexes are rare. Examples include a sill complex on the Béata Ridge (Révillon *et al.*, 2000) and a series of layered mafic–ultramafic intrusions on parts of the mainland in Colombia and Ecuador (Nivia, 1996; Kerr *et al.*, 1997*a*, 1997*b*; Lapierre *et al.*, 2000) and on Gorgona Island (Gansser, 1950; Gansser *et al.*, 1979; Echeverria, 1980; Aitken & Echeverria, 1984; Kerr *et al.*, 1996).

Gorgona Island

Gorgona is a small island, 8 km long and 2·5 km wide, located ~60 km off the Colombian Pacific coast (Fig. 1). The geology of the island has been studied by Gansser (1950), Gansser *et al.* (1979), Echeverria (1980), Aitken & Echeverria (1984) and Kerr *et al.* (1996), who have described an axial ridge of cumulate peridotites surrounded by sequences of ultramafic to mafic intrusive rocks. Volcanic rocks, which line the coast, are predominantly basaltic with intercalated komatiite. A large region of picritic volcanoclastic rocks forms the southern end of the island. These volcanic rocks are locally intruded by gabbros. The lava flows are flat lying and dips in bedded portions of the fragmental rocks rarely exceed 10°. Exposed contacts between different rock units are fault bounded. The island was previously described by Gansser (1950), Gansser *et al.* (1979) and Echeverria (1980) as a succession of tilted and faulted blocks, but preliminary studies of several seismic profiles to the west and east of the island suggest it could represent the summit of a ramp anticline linked to thrusting towards the NW (P. R. Cobbold, personal communication, 1999). All previous studies have focused on the volcanic rocks and no systematic work has been carried out on the intrusive rocks.

FIELD RELATIONS AND SAMPLE DESCRIPTIONS

Because of dense jungle cover, field observations and sampling were carried out only along the coast. Volcanic

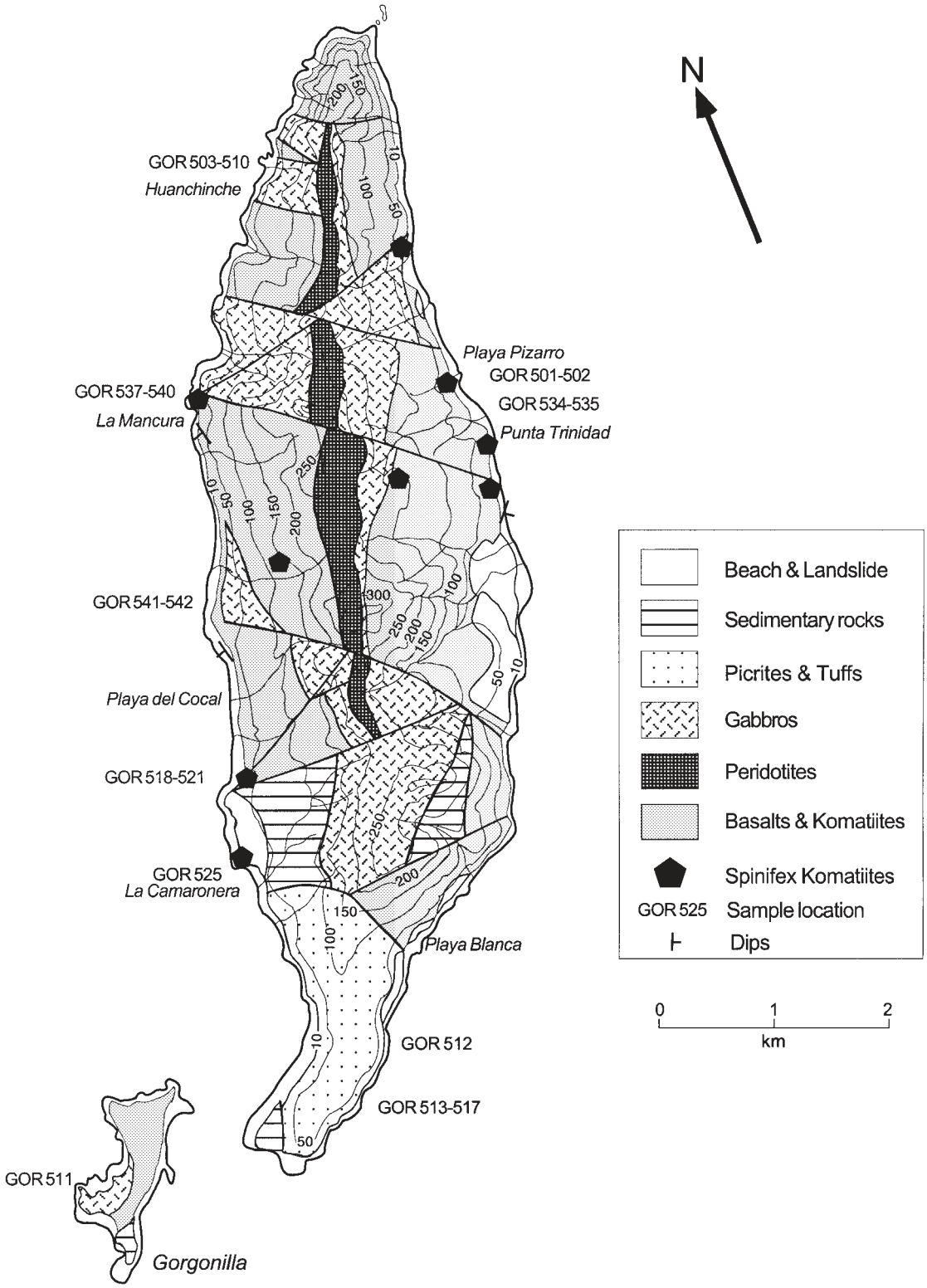

Fig. 1. Geological map of Gorgona Island [modified from Echeverria (1980)]. Numbers indicate the main sampling localities referred to in the text.

rocks and several gabbroic units were sampled from outcrops at the localities indicated in Fig. 1, and all samples of ultramafic intrusive rocks were obtained from boulders in the beds of small streams. Because the maximum length of these streams is <1 km, the source of the samples is well constrained. Rare outcrops in the interior of the island were described by Echeverria (1980) but were not sampled during this study.

Volcanic rocks: komatiites, komatiitic basalts and picrites

Detailed descriptions of komatiite flows have been given by Echeverria (1980) and Kerr *et al.* (1996). Four localities were sampled during this study. The first is Punta Trinidad on the east coast, where the komatiites are best exposed (Fig. 1, GOR 501 and 502). Three additional komatiite localities were sampled on the west coast (Fig. 1). At most of these locations only blocks (up to several metres in size) of spinifex-textured komatiite were found (La Camaronera, GOR 525; and south of Playa del Cocal, GOR 519–521) but at La Mancura (GOR 537–540) a sequence of alternating komatiitic and basaltic flows was sampled.

The picritic fragmental rocks were studied by Echeverria & Aitken (1986), who described in detail their volcanic structures and textures as well as their mineralogical and chemical compositions. These rocks, which are exposed only on the southern part of the island (Fig. 1), consist of tuffs and breccias containing numerous blocks of massive picrite (from a few centimetres to >1 m) in a matrix of finer-grained, highly altered material. Variations in the size and abundance of these blocks, which are rounded to angular, define a crude subhorizontal bedding. On the east coast, the fragmental rocks are intruded by picrite dykes up to 5 m wide. In a wave-cut platform exposure ~500 m north of the southern tip of the island, the termination of one such dyke was observed. The contact between massive picrite and the fragmental rocks is sharp and clearly intrusive in places, but highly irregular, and with no obvious chilling. In other places, fractures directed inward from the margins divide the dyke into numerous cells of massive picrite (from 1 to 20 cm in size) each surrounded by altered material that closely resembles the enclosing fragmental rock. In these regions the margins of the massive picrite dyke, sampled as GOR 512, appears to have disintegrated into fragmental rock. Echeverria & Aitken (1986) described these rocks as pyroclastic lapilli tuffs and tuff breccias, but in view of the relationships described above, and the similarity between these outcrops and sequences described by Smith & Batiza (1989) and Francis (1993), it is more probable that they formed as hyaloclastites. The picritic dykes are believed to represent intrusions into the breccias of the magma parental to the fragmental rocks.

On the west coast no dykes or blocks of massive picrites were observed, and the ultramafic fragmental rocks appeared to grade into sequences of immature sedimentary rocks that contain a high volcaniclastic component. It is possible that the site of eruption of the picritic hyaloclastites was to the SE and that the extent of sedimentary reworking increases to the NW.

In this study, we sampled several dykes and blocks of massive picrite. Only the freshest material, from the interior of dykes (GOR 512, GOR 515–517) and from massive blocks in the hyaloclastites (GOR 513 and 514), were analysed.

Intrusive rocks

Gabbros were sampled at four localities on both sides of the main island and also on Gorgonilla, a small island to the SW (Fig. 1). In none of these localities were contacts between gabbros and volcanic rocks observed and we have little idea of the overall size and form of the intrusive bodies. The largest outcrops, which are several hundred metres across, consist of relatively homogeneous, massive, olivine-free gabbro (GOR 510, 511 and 541). Olivine-bearing gabbros were not observed in outcrop but were sampled in boulders in stream beds (GOR 508, 509, 518, 534 and 535).

Ultramafic plutonic rocks were sampled at two locations on the west coast, at Huanchinche (GOR 503–507) and north of Playa del Cocal (GOR 542). All samples were from large boulders (up to 1–2 m) in small streams. Gabbros and olivine gabbros (GOR 508–510, GOR 541) were found in the same localities, but the contacts between the different rock types were not observed. Samples GOR 503–505 and GOR 542 are dunites and samples GOR 506 and 507 are wehrlites.

PETROGRAPHY AND MINERAL COMPOSITIONS

Detailed descriptions of the petrography and mineralogy of Gorgona komatiites and picrites have been given by Echeverria (1980, 1982), Aitken & Echeverria (1984), Echeverria & Aitken (1986) and Kerr *et al.* (1996), and will not be repeated here. Our new microprobe results are in agreement with previously published data from Gorgona komatiites and picrites. Representative mineral compositions are reported in Table 1 and olivine compositions are plotted in Fig. 2. The petrography and mineralogy of the intrusive rocks is summarized in Table 2.

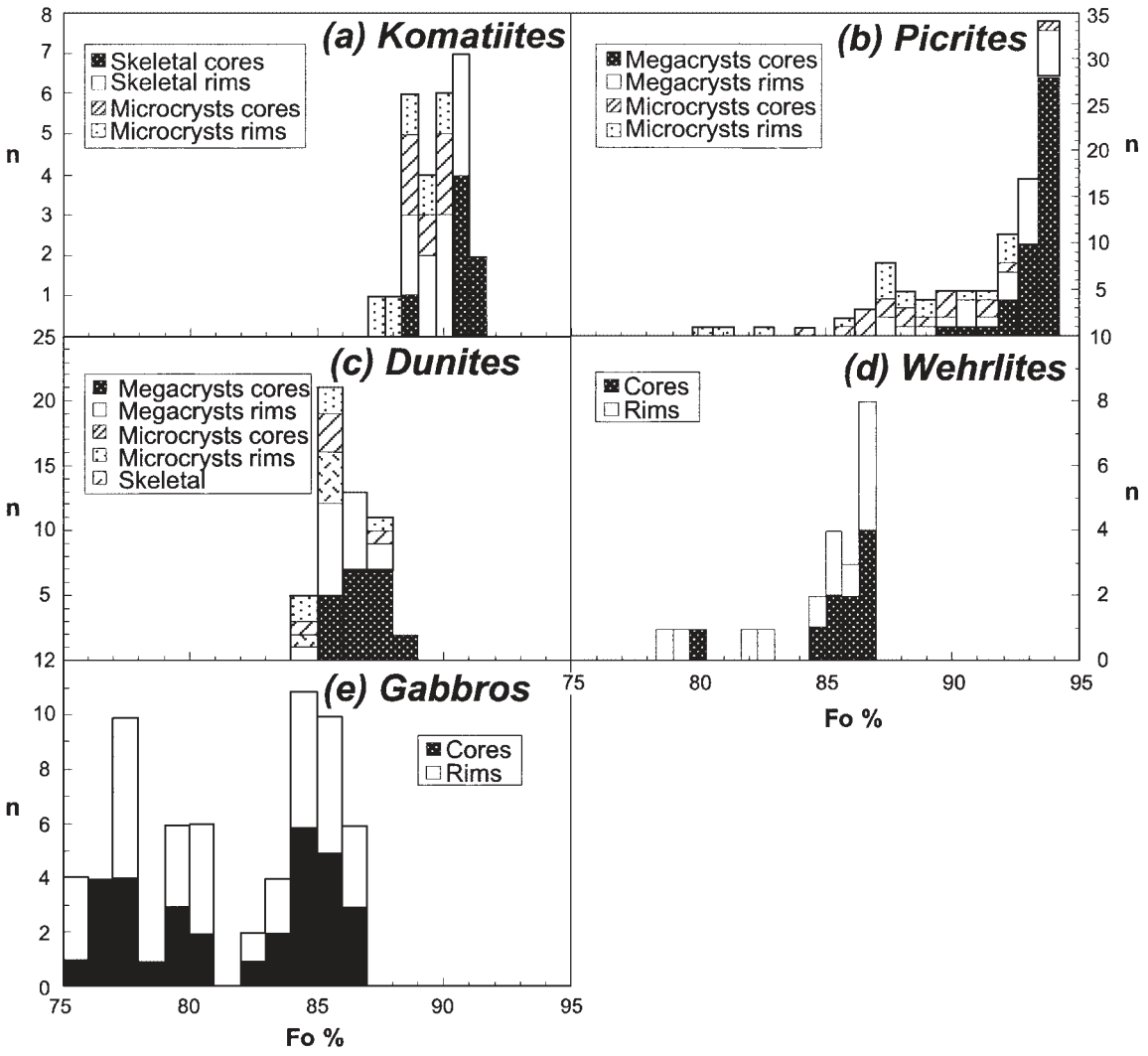

Fig. 2. Frequency histograms of olivine compositions (Fo %) from (a) komatiites, (b) picrites, (c) dunites, (d) wehrlites and (e) olivine gabbros. Frequency histograms are calculated for each olivine habit and for cores and rims of individual olivine grains. *n*, number of analyses.

The gabbros are coarse grained and have ophitic textures (GOR 508, Fig. 3a). Olivine, where present, forms euhedral grains up to 2 mm across. Other major phases are clinopyroxene, which occurs as large (up to 5 mm), anhedral grains, and plagioclase, which forms elongate, euhedral to subhedral grains (1 mm × 0·2 mm). Accessory phases are chromite and ilmenite. Small euhedral plagioclase grains are enclosed in anhedral clinopyroxene crystals, which suggests that plagioclase crystallized before pyroxene.

Dunites display a wide range of olivine morphologies. The dominant type, which forms 40–50% of all olivine grains, consists of large (up to 2 mm) polyhedral grains. These commonly display embayments that are interpreted either as corrosion gulfs or as growth features. A second type, which also comprises 40–50% of the olivine population, consists of much smaller (0·2 mm on average) rounded grains. Rare skeletal crystals were observed in some samples. Some are highly elongated (GOR 504, Fig. 3c) others are roughly equigranular (GOR 503, Fig. 3b). Olivine compositions fall in a narrow range from Fo_{84} to Fo_{88} and are identical for all habits (Table 1 and Fig. 2). Small amounts of poikilitic clinopyroxene, subhedral plagioclase and euhedral chromite were also observed.

Wehrlites are made up of 3 mm euhedral olivine grains and similar-sized anhedral to subhedral clinopyroxene crystals (GOR 506, Fig. 3d). Minor interstitial euhedral to subhedral plagioclase is also observed, as well as small skeletal grains of ilmenite and chromite.

All the intrusive rocks have been affected by hydrothermal alteration. Up to 10 vol. % of olivine is

Table 1: Selected micoprobe analyses of olivine from Gorgona Island rocks

Sample:	GOR 525	GOR 538	GOR 509	GOR 542	GOR 503	GOR 506	GOR 517
Rock type:	Komatiite	Komatiite	Ol-gabbro	Dunite	Dunite	Wehrlite	Picrite
Location:	Core	Core	Core	Core	Core	Core	Core
	Microcryst	Skeletal	Megacryst	Megacryst	Microcryst	Megacryst	Microcryst
SiO_2	41·04	41·70	40·93	40·70	40·37	40·10	41·25
Al_2O_3	0·11	0·08	0·03	0·08	0·16	0·02	0·05
TiO_2	0·01	0·01	—	0·02	0·01	0·04	0·00
Cr_2O_3	0·10	0·10	0·02	0·01	0·27	0·05	0·16
FeO*	9·64	8·51	12·87	12·05	12·49	13·02	6·17
MnO	0·15	0·17	0·23	0·20	0·17	0·26	0·08
MgO	50·38	51·44	47·58	47·73	47·61	47·46	51·37
CaO	0·31	0·30	0·30	0·34	0·23	0·36	0·28
Na_2O	0·01	0·01	0·02	—	—	—	0·02
K_2O	0·01	0·02	—	—	0·01	0·02	—
NiO	0·43	0·41	0·26	0·32	0·30	0·28	0·41
Total	102·19	102·75	102·28	101·48	101·62	101·61	99·79
Fo (%)	90·31	91·51	86·83	87·60	87·17	86·66	93·69

Analyses were carried at the University of Leicester on a JEOL 8600 and at Ifremer, Brest, on a CAMECA SX50 using time counting of 6 min and 36 s, respectively.

Table 2: Summary of the petrographic characteristics for Gorgona Island intrusive rocks

Rock type:	Gabbros	Dunites (ol-cumulates)	Wehrlites (ol-cpx cumulates)
Texture:	Coarse-grained ophitic	Granular	Coarse-grained
Grain size:	1–5 mm	0·2–2 mm	2–5 mm
Primary minerals			
	Olivine (0–25%)	Olivine (>90%)	Olivine (60–80%)
	Plagioclase (35–55%; $An_{88–38}$)	Plagioclase (~1%)	Clinopyroxene (20–40%; augite)
	Clinopyroxene (30–50%; augite)	Clinopyroxene (~5%; augite)	Plagioclase (<5%; $An_{70–55}$)
	Chromite, ilmenite	Chromite	Chromite, ilmenite
Secondary minerals			
	Serpentine (up to 10%; replacing olivine)	Serpentine (up to 10%; replacing olivine or in the groundmass)	Serpentine (5–10%; replacing olivine)
	Saussurite (up to 5%; replacing plagioclase)		Saussurite (replacing plagioclase)

serpentinized and plagioclase is saussuritized. Clinopyroxene is generally unaffected and no secondary amphiboles were observed. Small fractures in the ultramafic rocks are filled with serpentine but such fractures were not seen in the gabbros, which are generally less altered. No secondary minerals such as carbonates, phlogopite or talc were recognized either in volcanic or intrusive rocks. Although the LOI (loss on ignition; Table 3) of

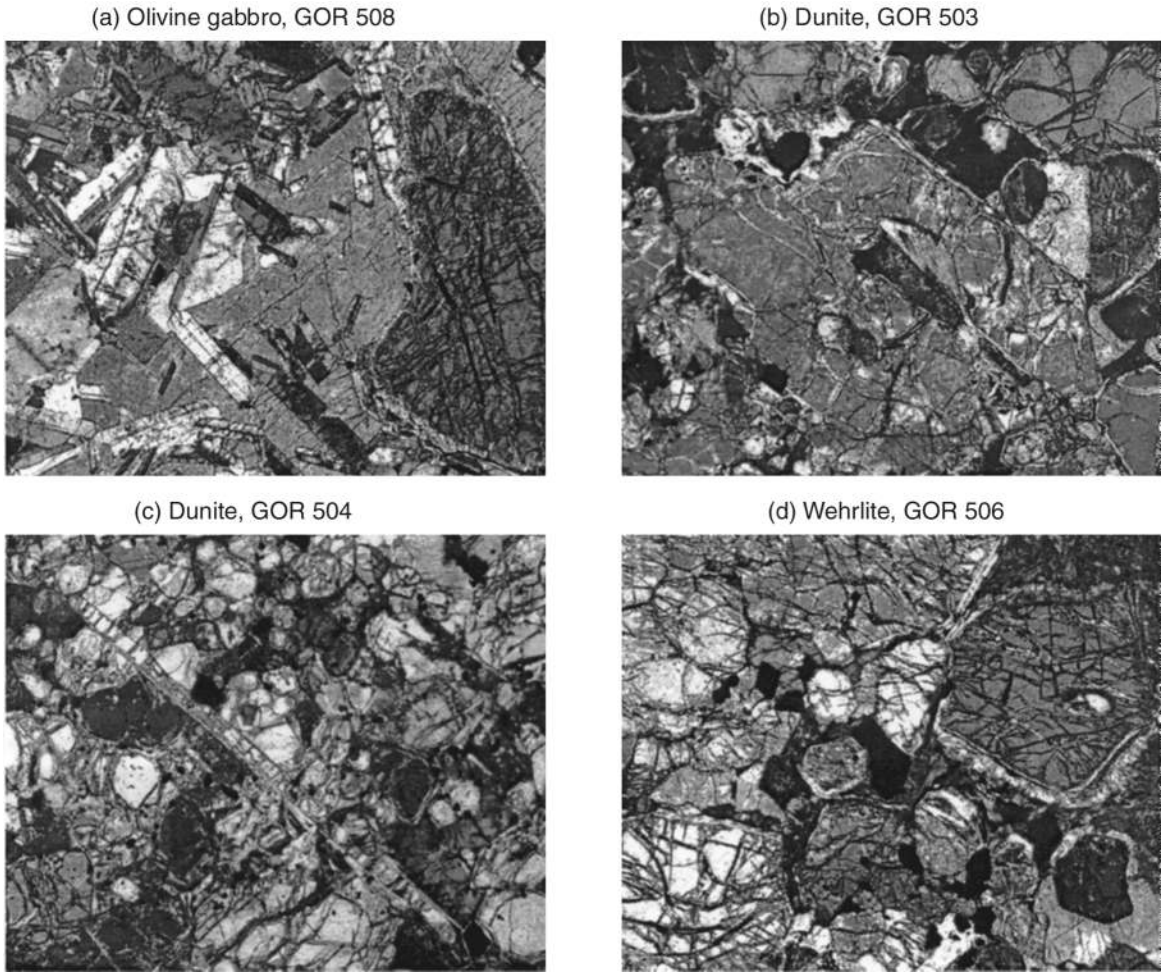

Fig. 3. Photomicrographs of plutonic rocks from Gorgona Island. All photographs were taken in crossed-polarized light. The width of the photo represents 5 mm. (a) Coarse-grained olivine gabbro GOR 508. (b) Skeletal olivine in dunite GOR 503. The bimodal distribution of olivine grains can be observed. (c) Needle-shaped olivine crystal in dunite GOR 504. (d) Coarse-grained wehrlite GOR 506.

most samples is high, the absence of such secondary minerals suggests that the original compositions are well preserved.

CHEMICAL COMPOSITIONS

Analytical techniques

Samples were powdered in agate mills. X-ray fluorescence (XRF) analyses were carried out at the University of Rennes. Major elements were determined on fused discs with estimated errors of <2% except for the minor oxides (5–10%); trace elements were measured on pressed powder pellets with a precision of 2% for elements with concentrations >100 ppm and ~10% for elements with 10–100 ppm. Other trace elements, including the rare earth elements (REE), were determined by inductively coupled plasma-mass spectrometry (ICP-MS) at the University of Montpellier on a VG-PQ^{2+}. About 100 mg of sample were dissolved in Teflon beakers using a 3:1 mixture of 24 M HF and $HClO_4$, followed by a mixture of 4:1 24 M HF and 14 M HNO_3. Analyses of standards BHVO and BIR-1 are within 5% of the recommended values. Because of the unusual compositions of Gorgona rocks, a komatiite standard (M664) was measured. It gave results within 5% of values obtained by spark-source mass spectrometry (Lahaye, 1995).

Neodymium isotopic compositions were measured on a Finnigan-MAT 262 at the University of Rennes. Blanks for Nd were <200 pg. Concentrations of Nd and Sm were determined in static mode using the $^{149}Sm/^{150}Nd$ total spike technique whereas Nd isotopic compositions were determined in triple-peak-jumping mode using the same sample load as for the concentration determination. The procedure gave a $^{143}Nd/^{144}Nd$ value of 0·511863 (average of 17 analyses) for the 'in house' standard, which corresponds to a value of 0·511856 for the La Jolla standard.

Table 3: Major (in wt %) and trace element (in ppm) analyses of Gorgona samples

Sample:	GOR 501	GOR 502	GOR 519	GOR 521	GOR 525	GOR 537	GOR 538	GOR 539
Rock type:	Komatiite	Komatiite	Komatiite	Komatiite	Komatiite	Komatiite	Komatiite	Komatiite
SiO_2	44·65	46·07	46·9	47·89	44·56	44·7	43·65	44·5
Al_2O_3	10·11	13·08	12·6	13·22	11·17	11·62	8·72	10·55
Fe_2O_3	12·57	12·64	11·76	11·72	12·7	12·65	11·79	12·17
FeO(T)	11·3	11·37	10·57	10·54	11·42	11·37	10·6	10·94
MnO	0·19	0·2	0·19	0·18	0·2	0·19	0·18	0·19
MgO	22·08	14·53	15·58	14·44	20·11	17·31	26·48	20·98
CaO	8·91	11·38	10·62	10·34	9·88	10·68	8·01	10·05
Na_2O	0·81	1·26	1·25	1·53	0·68	2·08	0·59	0·85
K_2O	0·02	0·04	0·59	0·16	0·03	0·06	0·03	0·05
TiO_2	0·61	0·74	0·48	0·49	0·64	0·66	0·51	0·62
P_2O_5	0·03	0·04	0·03	0·03	0·04	0·05	0·04	0·04
LOI	3·77	3·28	5·08	4·49	5·19	1·7	2·72	5·56
mg-no.	77·69	69·5	72·43	70·95	75·85	73·07	81·65	77·36
Ni	*1091*	*520*	*540*	*573*	*956*	*776*	*1519*	*1039*
Cr	*1717*	*1076*	*1134*	*1326*	*5614*	*1558*	*2935*	*1297*
Y	*12*	*15*	*14*	*14*	*12*	*14*	*11*	*12*
Co	*86*	*69*	*70*	*78*	*80*	*76*	*90*	*81*
V	*204*	*253*	*241*	*242*	*162*	*241*	*158*	*207*
Ga	*11*	*14*	*10*	*11*	*12*	*13*	*9*	*11*
Cu	*97*	*121*	*95*	*148*	*99*	*113*	*81*	*94*
Zn	*67*	*69*	*72*	*61*	*66*	*74*	*62*	*63*
Rb	0·69	0·93	3·51	1·27	1·17	0·87	0·61	0·61
Sr	44·17	58·5	207·82	108	66·39	108·57	40·21	91·14
Zr	*25*	*32*	*18*	*18*	*28*	*30*	*22*	*27*
Zr	24·11	30·84	16·62	16·05	24·81	28·65	20·62	25·07
Nb	0·35	0·45	0·28	0·28	0·38	0·42	0·3	0·37
Cs	0·01	0·02	0·02	0·04	0·01	0·01	0·01	0·01
Ba	2·17	3·02	733·52	136·6	2·74	5·94	1·49	7·75
La	0·49	0·66	0·33	0·31	0·53	0·63	0·43	0·52
Ce	1·85	2·32	1·05	1·06	1·92	2·19	1·49	1·94
Pr	0·36	0·48	0·22	0·22	0·39	0·45	0·31	0·39
Nd	2·39	3·09	1·52	1·52	2·52	2·87	1·98	2·54
Sm	1·08	1·4	0·84	0·84	1·15	1·32	0·91	1·16
Eu	0·5	0·65	0·35	0·39	0·53	0·6	0·41	0·51
Gd	1·77	2·34	1·81	1·69	1·86	2·14	1·51	1·86
Tb	0·32	0·43	0·33	0·33	0·34	0·39	0·28	0·33
Dy	2·24	3·01	2·52	2·46	2·37	2·73	1·92	2·3
Ho	0·47	0·62	0·56	0·55	0·49	0·56	0·4	0·48
Er	1·29	1·74	1·57	1·56	1·36	1·57	1·13	1·31
Tm	0·18	0·24	0·23	0·22	0·19	0·22	0·16	0·18
Yb	1·13	1·49	1·50	1·47	1·19	1·35	0·96	1·14
Lu	0·18	0·24	0·23	0·23	0·19	0·21	0·16	0·18
Hf	0·79	1·04	0·61	0·59	0·83	0·95	0·68	0·82
Ta	0·03	0·03	0·02	0·02	0·03	0·03	0·02	0·03
Pb	0·19	0·18	0·11	0·12	0·15	0·69	0·13	0·09
Th	0·04	0·04	0·02	0·03	0·03	0·03	0·02	0·03
U	0·02	0·02	0·01	0·01	0·01	0·01	0·01	0·01

Sample:	GOR 520	GOR 512	GOR 513	GOR 514	GOR 515	GOR 517	GOR 503	GOR 504
Rock type:	Komatiitic basalt	Picrite	Picrite	Picrite	Picrite	Picrite	Dunite	Dunite
SiO_2	48·22	45·27	45·36	45·93	44·46	44·58	41·88	41·87
Al_2O_3	14·84	9·76	9·98	10·3	8·71	8·5	5·03	5·16
Fe_2O_3	11·89	11·12	11·21	11·18	10·95	10·94	12·46	12·41
FeO(T)	10·69	10	10·08	10·05	9·84	9·84	11·2	11·16
MnO	0·19	0·18	0·18	0·18	0·17	0·18	0·18	0·18
MgO	9·51	24·44	23·54	22·74	27·29	27·87	35·41	34·65
CaO	13·01	8·21	8·68	8·5	7·73	7·24	4·67	5·42
Na_2O	1·69	0·66	0·66	0·63	0·37	0·33	0·13	0·1
K_2O	0·04	0·07	0·05	0·17	0·02	0·03	0·01	n.d.
TiO_2	0·55	0·3	0·33	0·34	0·27	0·32	0·22	0·21
P_2O_5	0·04	0·02	0·01	0·03	0·02	0·02	0·01	0·01
LOI	1·81	3·31	3·52	3·81	5·42	6·82	5·34	4·72
mg-no.	61·32	81·33	80·62	80·12	83·17	83·47	84·93	84·7
Ni	*165*	*1173*	*1116*	*1142*	*1318*	*1322*	*1889*	*1866*
Cr	*422*	*2105*	*2119*	*2322*	*2822*	*1542*	*4773*	*4590*
Y	*18*	*12*	*11*	*12*	*10*	*8*	*4*	*5*
Co	*53*	*84*	*82*	*82*	*89*	*89*	*21*	*19*
V	*276*	*162*	*170*	*171*	*135*	*148*	*84*	*86*
Ga	*14*	*9*	*9*	*9*	*8*	*7*	*5*	*6*
Cu	*140*	*71*	*79*	*74*	*56*	*43*	*37*	*27*
Zn	*67*	*64*	*62*	*64*	*60*	*60*	*64*	*64*
Rb	0·39	1·76	1·37	2·04	0·56		0·36	
Sr	73·61	23·78	17·55	29·01	15·53	*23*	*42·76*	*31*
Zr	*25*	*12*	*13*	*13*	*11*	*13*	*7*	*8*
Zr	21·29	9·34	11·04	11·38	9·54		6·79	
Nb	0·39	0·08	0·11	0·13	0·12	*0·3*	0·12	*0·2*
Cs	0·01	0·02	0·01	0·04	n.d.		0·01	
Ba	95·59	4·77	0·65	9·23	0·66	*9*	6	*10*
La	0·42	0·08	0·12	0·15	0·15		0·15	
Ce	1·44	0·33	0·42	0·55	0·46		0·43	
Pr	0·29	0·08	0·11	0·13	0·11		0·09	
Nd	1·93	0·67	0·81	0·91	0·77		0·59	
Sm	1·04	0·48	0·57	0·55	0·45		0·34	
Eu	0·49	0·27	0·3	0·28	0·23		0·16	
Gd	2·03	1·14	1·3	1·2	1		0·67	
Tb	0·4	0·24	0·27	0·25	0·21		0·13	
Dy	2·98	1·91	2·09	1·98	1·69		0·96	
Ho	0·67	0·43	0·48	0·46	0·39		0·21	
Er	1·87	1·28	1·37	1·35	1·18		0·59	
Tm	0·27	0·19	0·2	0·21	0·18		0·09	
Yb	1·8	1·18	1·29	1·32	1·12		0·53	
Lu	0·28	0·19	0·21	0·22	0·19		0·09	
Hf	0·75	0·35	0·41	0·4	0·35		0·25	
Ta	0·03	0·01	0·01	0·01	0·01		0·01	
Pb	0·1	0·05	0·07	0·07	0·07		0·08	
Th	0·03	0·01	0·01	0·01	0·01		0·02	
U	0·01	n.d.	n.d.	n.d.	n.d.		0·01	

Table 3: continued

Sample:	GOR 505	GOR 542	GOR 506	GOR507	GOR 508	GOR 509	GOR 518	GOR 534
Rock type:	Dunite	Dunite	Wehrlite	Wehrlite	Olivine gabbro	Olivine gabbro	Olivine gabbro	Olivine gabbro
SiO_2	41·7	42·85	43·25	43·03	45·98	44·04	44·96	47·93
Al_2O_3	5·37	6·81	6·52	6·9	18·45	8·15	10·12	16·25
Fe_2O_3	12·31	11·79	14·86	12·73	9·74	12·48	12·08	9·82
FeO(T)	11·06	10·6	13·36	11·45	8·76	11·23	10·86	8·83
MnO	0·18	0·17	0·23	0·19	0·16	0·22	0·2	0·15
MgO	34·2	31·5	27·6	29·63	11·14	27·2	22·21	9·4
CaO	5·94	6·28	6·5	7·21	12·62	7·4	9·38	13·88
Na_2O	0·07	0·26	0·22	n.d.	1·34	0·19	0·66	1·7
K_2O	0·01	0·01	0·02	n.d.	0·09	0·03	0·02	0·03
TiO_2	0·21	0·31	0·74	0·29	0·45	0·28	0·34	0·76
P_2O_5	0·01	0·01	0·04	0·01	0·03	0·02	0·02	0·06
LOI	5·44	4·74	4·74	7·16	3·09	6·36	3·62	2·47
mg-no.	84·64	84·11	78·64	82·18	69·39	81·2	78·47	65·49
Ni	*1845*	*1672*	*1239*	*1191*	*306*	*1180*	*929*	*186*
Cr	*4958*	*5594*	*957*	*2084*	*357*	*3940*	*1883*	*704*
Y	*4*	*7*	*11*	*7*	*10*	*7*	*10*	*13*
Co	*12*	*106*	*14*	*14*	*56*	*3*	*89*	*43*
V	*88*	*97*	*204*	*131*	*175*	*125*	*168*	*237*
Ga	*5*	*6*	*9*	*7*	*14*	*8*	*9*	*16*
Cu	*37*	*54*	*62*	*48*	*100*	*74*	*70*	*120*
Zn	*66*	*62*	*79*	*69*	*59*	*91*	*65*	*59*
Rb	0·23	0·32	0·66	0·16	1	0·62		0·43
Sr	19·75	25·37	21·07	4·89	90·23	10·82	*54*	102·77
Zr	*8*	*12*	*26*	*10*	*20*	*8*	*12*	*39*
Zr	6·77	10·79	27·88	8·63	17·02	7·67		33·72
Nb	0·11	0·19	0·71	0·15	0·4	0·2	*0·7*	2·58
Cs	n.d.	0·01	0·01	0·01	0·01	0·01		0·01
Ba	3·92	4·33	2·56	0·84	9·36	1·28	*62*	15·58
La	0·13	0·23	0·73	0·15	0·45	0·21		2·14
Ce	0·39	0·72	2·48	0·48	1·42	0·63		5·57
Pr	0·09	0·15	0·48	0·11	0·29	0·12		0·83
Nd	0·57	1	3·07	0·74	1·88	0·76		4·24
Sm	0·34	0·53	1·28	0·43	0·87	0·39		1·5
Eu	0·17	0·25	0·53	0·22	0·43	0·21		0·65
Gd	0·69	1	1·9	0·86	1·46	0·78		2·16
Tb	0·14	0·2	0·33	0·17	0·27	0·16		0·38
Dy	1	1·44	2·24	1·25	1·91	1·25		2·59
Ho	0·22	0·31	0·46	0·27	0·4	0·29		0·53
Er	0·59	0·9	1·24	0·75	1·09	0·88		1·43
Tm	0·09	0·13	0·18	0·11	0·16	0·13		0·2
Yb	0·54	0·82	1·08	0·67	0·98	0·88		1·24
Lu	0·09	0·13	0·17	0·11	0·15	0·15		0·19
Hf	0·25	0·38	0·9	0·32	0·57	0·27		1·06
Ta	0·01	0·02	0·05	0·01	0·03	0·02		0·17
Pb	0·08	0·1	0·19	0·1	0·17	0·16		0·47
Th	0·01	0·02	0·05	0·01	0·03	0·02		0·19
U	n.d.	0·01	0·02	0·01	0·01	0·01		0·06

Sample:	GOR 535	GOR 510	GOR 511	GOR 541	GOR 541
Rock type:	Olivine gabbro	Gabbro	Gabbro	Gabbro	Duplicate
SiO_2	43·57	48·12	46·21	47·31	
Al_2O_3	8·56	15·31	18·47	15·16	
Fe_2O_3	14·53	12·56	11·83	12·89	
FeO(T)	13·07	11·29	10·64	11·59	
MnO	0·21	0·18	0·18	0·2	
MgO	24·13	7·53	8·14	7·97	
CaO	8·03	12·67	11·59	13·08	
Na_2O	0·28	2·59	2·64	2·37	
K_2O	0·03	0·05	0·05	0·07	
TiO_2	0·64	0·92	0·84	0·9	
P_2O_5	0·04	0·06	0·06	0·05	
LOI	5·1	2·26	4·52	2·53	
mg-no.	76·7	54·29	57·69	55·08	
Ni	*981*	*98*	*119*	*118*	
Cr	*2259*	*331*	*347*	*302*	
Y	*9*	*22*	*18*	*20*	
Co	*105*	*50*	*52*	*52*	
V	*171*	*335*	*288*	*328*	
Ga	*10*	*18*	*18*	*17*	
Cu	*76*	*153*	*114*	*150*	
Zn	*82*	*71*	*52*	*76*	
Rb	1·21	0·81	0·98	0·5	0·5
Sr	50·51	111·14	187·97	106·89	106·4
Zr	*25*	*42*	*36*	*42*	*42*
Zr	26·16	36·92	35·10	37·10	36·60
Nb	1·71	1·19	1·11	0·64	0·63
Cs	0·04	0·01	0·02	0·01	0·01
Ba	7·48	14·13	12·2	7·71	7·73
La	1·32	0·94	1	0·86	0·86
Ce	3·52	3·06	3·1	3·09	3·11
Pr	0·54	0·59	0·58	0·61	0·61
Nd	2·97	3·83	3·62	3·99	4
Sm	1·1	1·75	1·62	1·79	1·78
Eu	0·46	0·79	0·76	0·81	0·8
Gd	1·64	2·86	2·57	2·9	2·87
Tb	0·29	0·52	0·47	0·52	0·52
Dy	1·98	3·62	3·22	3·66	3·6
Ho	0·41	0·75	0·67	0·76	0·75
Er	1·09	2·05	1·86	2·06	2·05
Tm	0·16	0·29	0·26	0·29	0·29
Yb	0·98	1·81	1·65	1·81	1·81
Lu	0·16	0·28	0·26	0·28	0·28
Hf	0·82	1·21	1·14	1·26	1·22
Ta	0·11	0·08	0·08	0·05	0·05
Pb	0·17	0·09	0·14	0·07	0·07
Th	0·12	0·08	0·08	0·05	0·05
U	0·04	0·03	0·03	0·02	0·02

Major elements were measured by XRF; trace elements by XRF (italics) or ICP-MS (plain text). LOI, loss on ignition. *mg*-no. = Mg/[Mg + Fe(T)]. Major elements are reported on a volatile-free basis. n.d., not detected.

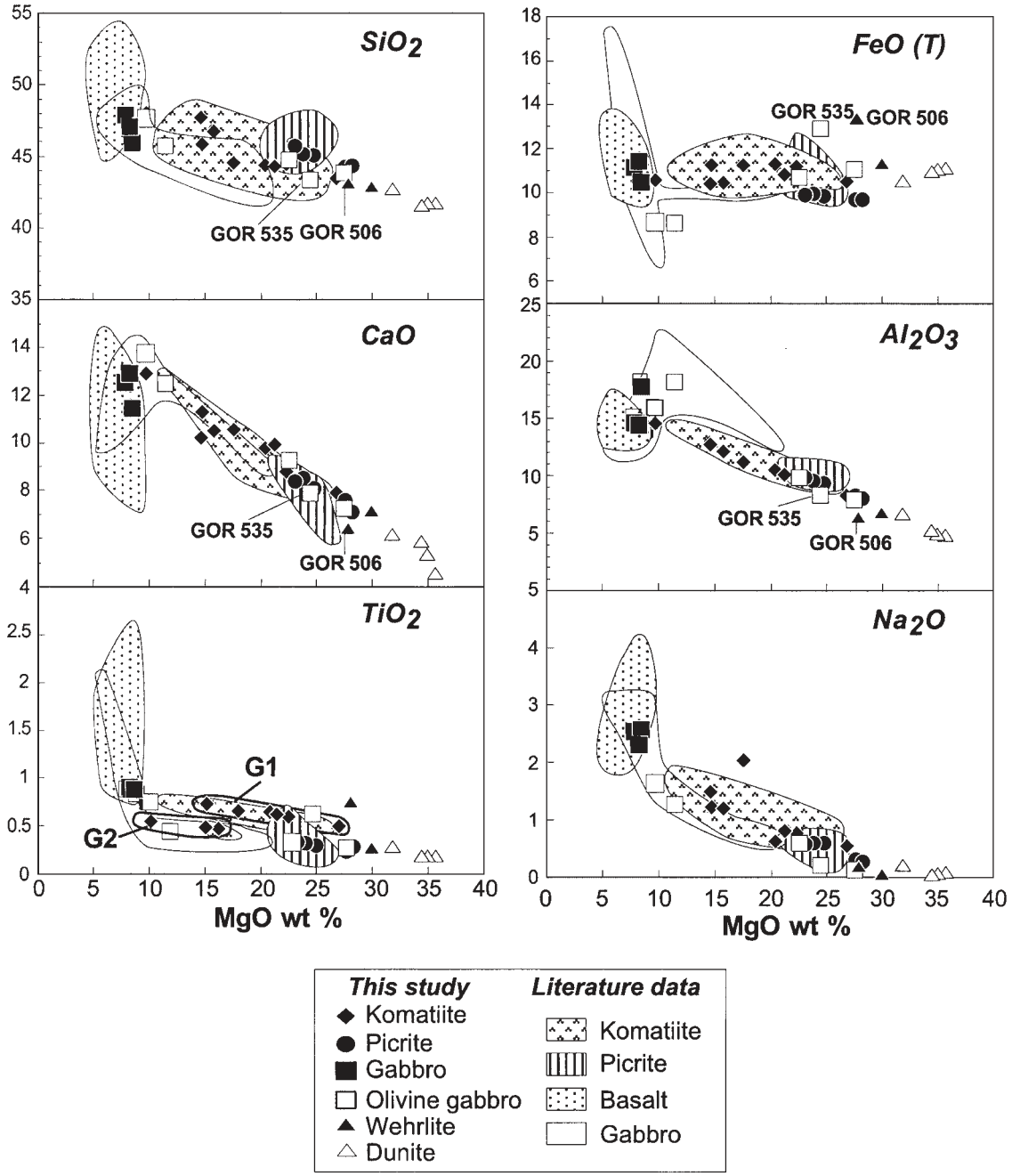

Fig. 4. MgO (wt %) vs SiO_2, CaO, TiO_2, $FeO_{(T)}$, Al_2O_3 and Na_2O (wt %) for the Gorgona rocks. Fe is reported as total Fe^{2+}. Fields are literature data from Echeverria (1980), Kerr *et al.* (1996), Arndt *et al.* (1997) and A. C. Kerr (unpublished data, 1998). The fields G1 and G2 identify the two komatiite groups.

Major elements

Major and trace element analyses of representative samples from each rock group are reported in Table 3 and plotted in Figs 4 and 5.

Komatiites and komatiitic basalts have MgO contents between 25 and 9 wt %. The major element characteristics of the new samples do not differ from those previously reported (Echeverria, 1980; Aitken & Echeverria, 1984; Kerr *et al.*, 1996; Arndt *et al.*, 1997). However, differences in minor elements such as TiO_2, when used in conjunction with incompatible trace elements, enable us to define two groups: G1 komatiites, which have relatively high abundances of TiO_2 and incompatible trace elements, and G2 komatiites, with

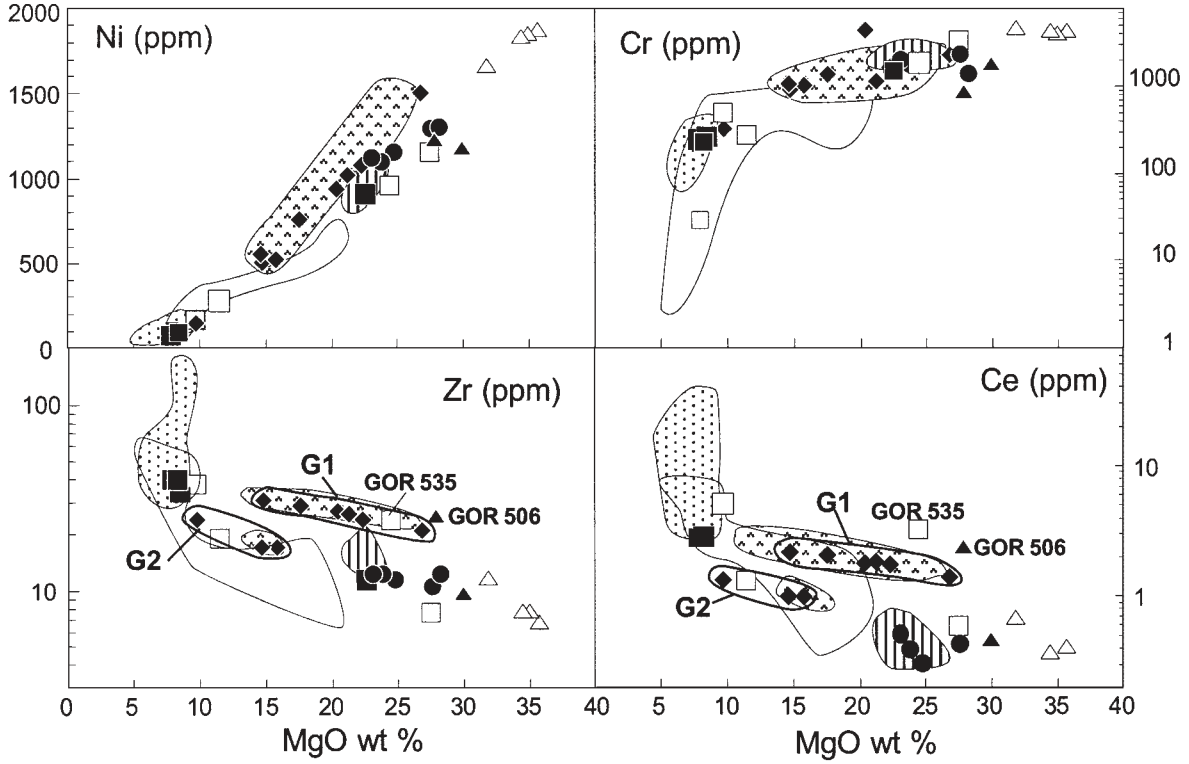

Fig. 5. MgO (wt %) vs Ni, Cr, Zr and Ce (ppm) for the Gorgona rocks. Sources of literature data are listed in Fig. 4. The fields G1 and G2 identify the two komatiite groups.

lower abundances (Figs 4 and 5). In the new dataset, picrites have higher MgO and lower $FeO_{(T)}$ contents compared with the komatiites (Fig. 4).

As seen in Fig. 4, the gabbros exhibit a large range of MgO contents, from 7 to 27 wt %. In terms of $FeO_{(T)}$, CaO, Al_2O_3, Na_2O and TiO_2, the three samples with high MgO contents lie in either the komatiite or the picrite field. The exception is sample GOR 535, which has higher $FeO_{(T)}$ than the others (Fig. 4). Two low-MgO olivine gabbros also plot close to the komatiite fields, except for Al_2O_3, which is higher, and $FeO_{(T)}$, which is lower. The other olivine-free gabbros plot within the fields defined by Gorgona basalts.

Wehrlites and dunites display the highest MgO contents, from ~35 wt % in dunites to ~30 wt % in wehrlites (Fig. 4). These samples have uniform major element characteristics, except for one wehrlite sample (GOR 506), which has a higher $FeO_{(T)}$ content. CaO, Al_2O_3, Na_2O and TiO_2 contents of both rock types are low.

Over the entire MgO range and for all rock types, SiO_2 increases and $FeO_{(T)}$ is almost constant. CaO and Al_2O_3 increase to reach a maximum at ~9 wt % MgO and then decrease slightly. Na_2O and TiO_2 increase for the entire MgO range, but show a break in the slope at ~9 wt % MgO (Fig. 4). These variations in major-element chemistry suggest that magma evolution is strongly influenced by fractionation and accumulation of olivine in the ultramafic rocks and by fractionation of plagioclase and clinopyroxene in the gabbros and associated basalts.

Trace elements

Selected trace element concentrations are plotted in Fig. 5 as a function of the MgO content. From dunites to gabbros, Ni and Cr decrease linearly with decreasing MgO, as would be expected from the fractionation or accumulation of olivine and minor chromite. As already noted by Echeverria & Aitken (1986), the Ni contents of picrites, both in whole rocks and in olivines, are lower than those of komatiites at given MgO contents. The accelerated decrease in Cr contents at ~10 wt % can be linked to clinopyroxene crystallization.

Zr and Ce are reported as examples of incompatible trace elements (Fig. 5). Both increase throughout the MgO range, from dunite to gabbro, but differences in the overall levels highlight the distinction between the two groups of komatiite. As already noted for major

elements, one wehrlite (GOR 506) and one olivine gabbro (GOR 535) display higher values.

Multi-element diagrams normalized to primitive mantle for all rock types are reported in Fig. 6. Almost all samples show depletion in the most incompatible elements, a negative Zr anomaly and variable scatter in the more mobile elements (Rb, Ba, Sr and Pb). Although Zr concentrations measured by ICP-MS are slightly lower than those measured by XRF, the agreement between the two sets of data is good and the presence of systematic negative Zr anomalies is thought to be a real feature of Gorgona rocks. The extent of depletion of incompatible elements increases from gabbro to picrite (La_N/Yb_N = 0·05–0·09). Light REE (LREE) patterns in gabbros and olivine gabbros are flat to moderately depleted (La_N/Yb_N = 0·91–1·17 to La_N/Yb_N = 0·31–0·41), and highly depleted in dunites and wehrlites (La_N/Yb_N = 0·15–0·19), except for one sample (GOR 506, La_N/Yb_N = 0·46). The two komatiite types are clearly distinguished; G1 komatiites have a humped pattern, being depleted in both LREE and heavy REE (HREE) whereas G2 komatiites are depleted in LREE but have flat HREE (Gd_N/Yb_N = 1·1–1·35 and 0·8–1·0, respectively).

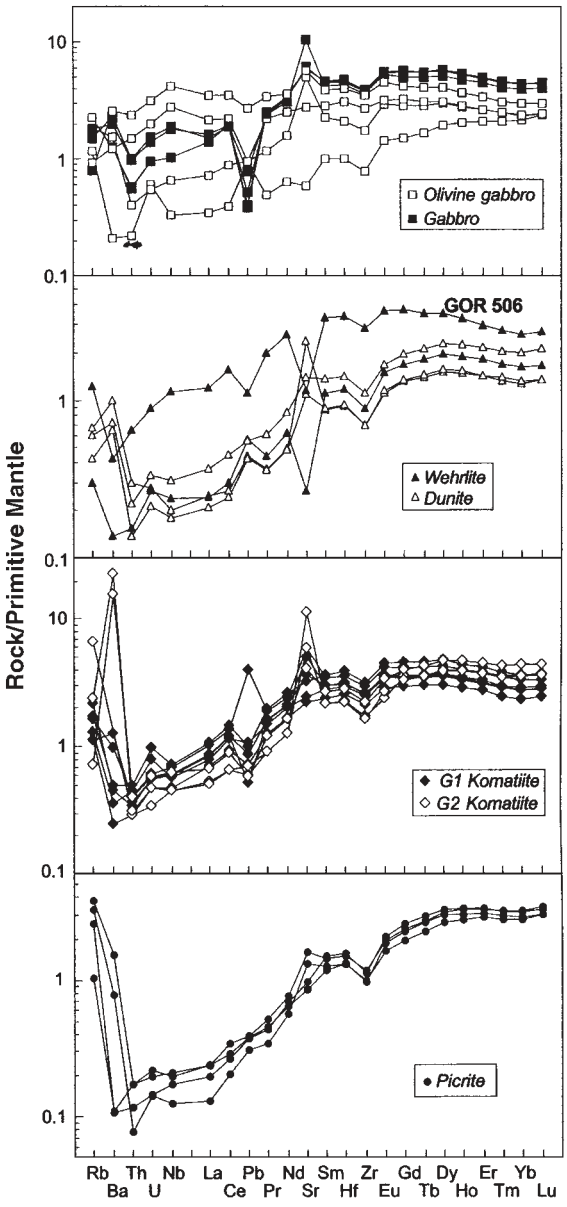

Fig. 6. Multi-element diagrams normalized to the primitive mantle abundances of Hofmann (1988) for Gorgona rocks.

Isotopic compositions

Neodymium isotopic compositions for representative samples are reported in Table 4. Initial Nd isotopic compositions are plotted in Fig. 7 as a function of $^{147}Sm/^{144}Nd$ ratios. All isotopic compositions suggest derivation of Gorgona magmas from a depleted mantle source with highly positive $\varepsilon_{Nd(T)}$. Two groups of magmatic rocks can be distinguished: a highly depleted group with $^{143}Nd/^{144}Nd_{(T)}$ >0·512947 (referred to as 'Group 1' in Fig. 7); and a less depleted group with $^{143}Nd/^{144}Nd_{(T)}$ from 0·512914 to 0·512794 ('Group 2' in Fig. 7). In both groups, $^{147}Sm/^{144}Nd$ ratios are highly variable, ranging from MORB-like values around 0·22 in two gabbros, to extremely high values of 0·46 in the most depleted picrites. All the komatiites, and all but one of the picrites, are found in the most depleted group, together with the majority of the intrusive rocks. However, one dunite (GOR 503), three gabbros (GOR 534, GOR 535 and GOR 509) and one picrite are found in the second group, together with E-basalts [enriched basalts as defined by Kerr *et al.* (1996)] and some of the D-basalts (depleted basalts). The fields of depleted Gorgona rocks are separate from the fields of MORB and Galapagos samples.

DISCUSSION

Emplacement mechanisms of the volcanic and plutonic rocks

The limited extent and poor quality of the outcrops prevented us from determining the relative volumes of the different types of intrusive rocks and their relative ages and relationships with the volcanic rocks. None the less, certain aspects of their textures, particularly of the dunites and wehrlites, provide important information about the conditions of emplacement. The most significant feature is the occurrence in several dunites (e.g. GOR 503 and GOR 504; Fig. 3b and c) of skeletal olivine grains and abundant small rounded crystals. Both forms suggest crystallization from silicate liquids, thus eliminating the possibility that these rocks are tectonically emplaced slices of upper-mantle peridotite. The skeletal

Table 4: Nd isotopic compositions for Gorgona rocks

Sample	Rock type	Nd	Sm	$^{147}Sm/^{144}Nd$	$^{143}Nd/^{144}Nd$	2σ	$^{143}Nd/^{144}Nd_{(T=88\,Ma)}$	εNd_0	εNd_t
GOR 501	Komatiite	2·89	1·38	0·2881	0·513194	4	0·513028	10·85	9·82
GOR 502	Komatiite	3·09	1·47	0·2874	0·513187	4	0·513022	10·71	9·69
GOR 519	Komatiite	1·55	0·85	0·3331	0·513197	6	0·513005	10·90	9·37
GOR 520	Komatiite	2·08	1·14	0·3314	0·513184	5	0·512993	10·65	9·14
GOR 521	Komatiite	1·6	0·9	0·3418	0·513213	5	0·513016	11·22	9·58
GOR 525	Komatiite	3·77	1·79	0·2869	0·513203	5	0·513038	11·02	10·01
GOR 537	Komatiite	4·45	2·13	0·289	0·513205	7	0·513039	11·06	10·02
GOR 538	Komatiite	2·3	1·09	0·2873	0·513209	6	0·513044	11·14	10·12
GOR 539	Komatiite	*2·54*	*1·16*	0·2747	0·513148	10	0·512990	9·95	9·07
GOR 94-07	Komatiite	1·91	1·06	0·3344	0·513167	13	0·512974	10·32	8·77
GOR 94-08	Komatiite	1·45	0·82	0·3404	0·513143	8	0·512947	9·85	8·23
GOR 94-28	Komatiite	2·15	1·01	0·2826	0·513167	6	0·513004	10·32	9·35
GOR 94-29	Komatiite	3·38	1·61	0·2889	0·513197	17	0·513031	10·90	9·87
GOR 94-30	Komatiite	2·67	2·29	0·51	0·513197	8	0·512903	10·90	7·38
GOR 94-41	Komatiite	3·9	1·87	0·2908	0·513205	10	0·513038	11·06	10·00
GOR 513	Picrite	0·91	0·67	0·4454	0·513300	11	0·513044	12·91	10·12
GOR 515	Picrite	0·84	0·51	0·3702	0·513257	7	0·513044	12·07	10·12
GOR 512	Picrite	*0·67*	*0·48*	0·4356	0·513311	6	0·513060	13·13	10·44
GOR 514	Picrite	*0·91*	*0·55*	0·3665	0·513213	4	0·513002	11·22	9·31
GOR 94-35	Picrite	0·99	0·75	0·4583	0·513239	8	0·512975	11·72	8·78
GOR 503	Dunite	*0·59*	*0·34*	0·3471	0·512994	10	0·512794	6·94	5·25
GOR 505	Dunite	0·58	0·34	0·3521	0·513194	15	0·512991	10·85	9·10
GOR 542	Dunite	0·97	0·52	0·3219	0·513196	5	0·513011	10·88	9·48
GOR 506	Wehrlite	3·67	1·59	0·2621	0·513160	11	0·513009	10·18	9·45
GOR 507	Wehrlite	0·84	0·51	0·3626	0·513192	4	0·512983	10·81	8·94
GOR 509	Olivine gabbro	0·83	0·45	0·3274	0·513053	4	0·512865	8·10	6·62
GOR 534	Olivine gabbro	4·38	1·58	0·2187	0·512995	5	0·512869	6·96	6·71
GOR 535	Olivine gabbro	3·1	1·18	0·2308	0·513047	4	0·512914	7·98	7·59
GOR 508	Olivine gabbro	*1·88*	*0·87*	0·2807	0·513142	4	0·51298	9·83	8·89
GOR 510	Gabbro	4·12	1·95	0·2925	0·513137	4	0·512969	9·73	8·66
GOR 511	Gabbro	3·89	1·77	0·2759	0·513159	4	0·513000	10·16	9·27
GOR 541	Gabbro	3·66	1·71	0·2821	0·513204	6	0·513042	11·04	10·08
GOR 94-05	Gabbro	1·98	0·93	0·2843	0·513190	6	0·513026	10·77	9·78
GOR 94-13	Gabbro	4·05	1·91	0·2851	0·513196	6	0·513032	10·88	9·89
GOR 94-13*	Gabbro	4·11	1·93	0·2842	0·513194	9	0·513030	10·85	9·86
GOR 94-14	Gabbro	4·61	2·02	0·2647	0·513159	6	0·513007	10·16	9·40
GOR 94-15	Gabbro	1·98	1·19	0·3643	0·513216	6	0·513006	11·28	9·39
GOR 94-16	Gabbro	5·33	2·51	0·285	0·513129	6	0·512965	9·58	8·58

Nd and Sm concentrations (in ppm) were analysed by isotopic dilution (plain text) or ICP-MS (italics). Major and trace element data for series 94 have been given by Kerr *et al.* (1996*a*) and Arndt *et al.* (1997).
*Duplicate analysis.

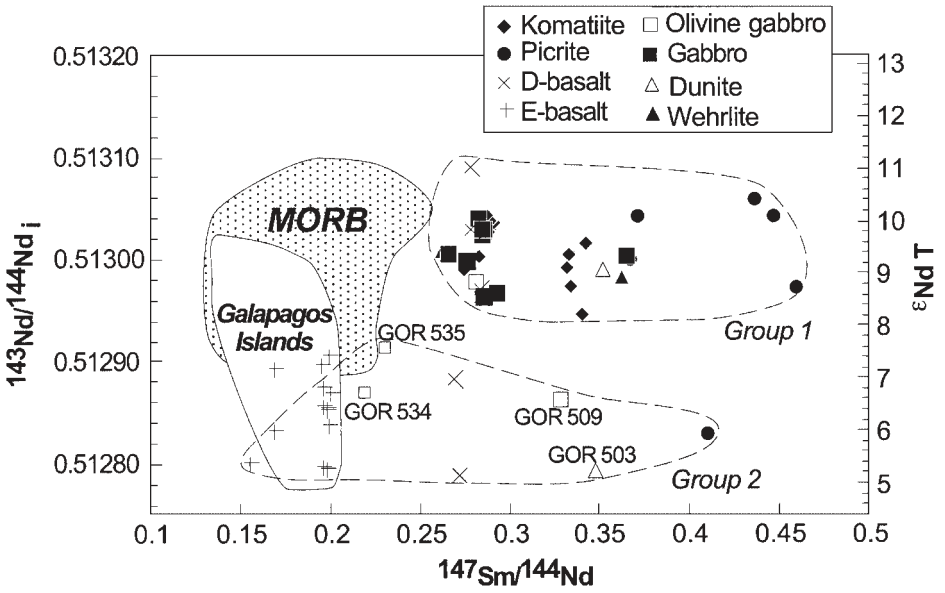

Fig. 7. $^{147}Sm/^{144}Nd$ vs $^{143}Nd/^{144}Nd_i$ of Gorgona rocks. The compositions of E- and D-basalts were published by Kerr *et al.* (1996) and Arndt *et al.* (1997). The picrite with a lower $^{143}Nd/^{144}Nd_i$ is from Arndt *et al.* (1997). Also shown for comparison are the fields of Pacific MORB (Cohen & O'Nions, 1982; White *et al.*, 1987) and Galapagos lavas (White *et al.*, 1993). The fields 'Group 1' and 'Group 2' identify the two groups of volcanic and intrusive rocks.

forms resemble those produced from ultramafic lavas in dynamic crystallization experiments and can be taken as evidence of rapid crystallization, probably caused by rapid cooling (Nesbitt, 1971; Donaldson, 1979). The abundant, small olivine crystals are similar to those at the margins of komatiite flows (Renner *et al.*, 1993) and are interpreted to indicate rapid nucleation from a supersaturated liquid, also a sign of rapid cooling. These indications of high cooling rates provide evidence that the dunites and wehrlites were emplaced in a cold environment. It is unlikely that they represent parts of differentiated lava flows, because all samples have cumulus or gabbroic textures and none display the distinctive quench textures that characterize the upper parts of differentiated komatiitic flows in Archaean greenstone belts (Arndt, 1986; Hill *et al.*, 1989). It is more probable that they formed as small intrusions within relatively cool wall rocks, perhaps a series of small sills emplaced at a high level in the volcanic pile.

Parental magma compositions, olivine fractionation and accumulation

The compositions of olivine phenocrysts were used to estimate the composition of the parental magma for each major rock type. In Fig. 8a and b, olivine compositions are plotted as a function of the MgO contents of the whole rocks. Also shown are curves representing the composition of olivine in equilibrium with liquids with 8, 9 and 10% FeO. These values correspond to the ferrous oxide content of likely parental magmas, as estimated from whole-rock compositions (Fig. 4), assuming ferric iron equals 15% of the total iron content of the magma. If the most magnesian olivine from a sample plots on an olivine–liquid equilibrium curve, this indicates that the MgO content of the whole rock is that of the liquid from which the olivine crystallized; if the olivine plots below the curves, this indicates that the rocks have accumulated olivine (Révillon *et al.*, 1999).

Both cases are represented by Gorgona rocks. The most magnesian olivines from the picrites and komatiites plot on the olivine equilibrium curves. For the picrites, the most magnesian olivine contains 93·6 forsterite and this composition plots close to the 9 wt % FeO curve (the value appropriate for these low-Fe rocks). From Fig. 4 we estimate that the MgO content of the parental liquid was ~25 wt %. There are several uncertainties associated with this estimate. The value chosen for the FeO content is subject to an error of ~1 wt %, as is the uncertainty on the proportion of ferric iron. Increasing the partition coefficient between olivine and the liquid to 0·33 (Bickle, 1982) would decrease the estimated MgO content by ~1 wt %. The total error on the estimate probably is close to ±2 wt %.

For both komatiite groups, olivine compositions plot close to the 10 wt % FeO curves and the MgO content of their parental magma is estimated at 20 ± 2 wt %. These calculations indicate that both picrites and komatiites were derived from highly magnesian liquids. In contrast, olivines from the intrusive rocks plot well

below the lines. This indicates that these rocks formed through the accumulation of olivine that had crystallized from less magnesian liquids. The most Fo-rich olivine from the dunite has only Fo_{88} indicating an MgO content for the parental liquid of 13 $\pm$ 2 wt %. In the same manner, the MgO content of the parental liquid of the wehrlites and olivine gabbros can be calculated at 12 wt % or less.

It is possible that the relatively low forsterite contents of olivines in the dunites result from re-equilibration with Fe-rich groundmass during cooling, as has been demonstrated for cumulates in the layered series of the Rum Intrusion in Scotland. Such an interpretation is consistent with the relatively narrow range of Fo contents, from Fo_{84} to Fo_{88}. If so, the olivine compositions cannot be used to estimate parental liquid compositions. However, several arguments can be made against re-equilibration. First, the relatively fine grain size and skeletal habits of olivine grains in the dunites indicate that they cooled rapidly, which would not have allowed time for significant re-equilibration. Second, the wehrlites, which are coarser grained and appear to have cooled more slowly than the dunites, display a larger range in olivine compositions (from Fo_{86} to Fo_{78}). Finally, as will be shown later in the paper, some of the basaltic lavas on Gorgona have trace-element ratios similar to those of komatiite lavas and to the intrusive dunites (Fig. 9 and following section). These rocks provide clear evidence of the existence of komatiite-derived basaltic liquids of the type we believe to have formed the dunitic intrusions.

Relationships between volcanic and plutonic rocks

To establish how the volcanic and intrusive rocks are related, their trace-element characteristics are compared in Fig. 9a and b. In both diagrams $(La/Sm)_N$ ratios are plotted against other incompatible element ratios. By plotting ratios, the effects of olivine fractionation or accumulation are minimized. It is evident from Fig. 9a and b that the Gorgona rocks form a semi-continuous series, from the extremely depleted picrites to the slightly enriched E-basalts. Focusing on relationships between intrusive and volcanic rocks, it appears that: (1) two of the gabbros have enriched trace-element characteristics similar to those of the E-basalts (referred to as enriched group in Fig. 9a and b); (2) a second group comprises the D-basalts, four gabbros and a wehrlite (referred to as depleted group in Fig. 9a and b); (3) a third group comprising the remaining gabbro, the dunites and a wehrlite has more depleted characteristics comparable with those of the komatiites (referred to as highly depleted group in Fig. 9a and b). None of the intrusive rocks have the extremely low ratios recorded in the picrites. The two groups of komatiites (G1 and G2) are readily distinguished in Fig. 9b, where $(La/Sm)_N$ is plotted against $(Gd/Yb)_N$. In terms of $(Gd/Yb)_N$, the gabbros and D-basalts resemble the less depleted G1 komatiites, whereas the dunites have ratios more like those of the more depleted G2 komatiites.

In general terms, the trace-element characteristics of most of the intrusive rocks resemble those of the komatiitic magma series and are distinct from both the basaltic lavas from Gorgona and from the dominant type of basalt throughout the Caribbean plateau, which have near-chondritic ratios of incompatible trace elements (Kerr *et al.*, 1997*b*; Sinton *et al.*, 1998; Révillon *et al.*, 1999, 2000; Hauff *et al.*, 2000). On the other hand, the liquids from which these rocks crystallized had basaltic compositions. It appears that the intrusive rocks were derived, in two separate stages, from liquids that were also parental to the komatiites and picrites. In the first stage these liquids were trapped at a deeper level in the crust where they differentiated through olivine fractionation to basaltic compositions; in the second stage the evolved liquids intruded into the volcanic pile where they underwent further differentiation and accumulated olivine and pyroxene.

To test this hypothesis, we first calculated the concentrations of all elements incompatible with olivine in the parental liquids of each rock type. This was done by projecting data plotted in variation diagrams along olivine control lines to the MgO contents of the parental liquids as calculated from the olivine compositions (Fig. 8). The results are shown in Figs 10 and 11. The procedure could not be used for the wehrlites, which contain a significant proportion of cumulus clinopyroxene.

Based on trace-element characteristics, we link the olivine gabbros to G1 komatiites (Fig. 10), and the dunites to G2 komatiites (Fig. 11). The calculated parental liquids of the gabbros could be derived from G1 komatiites by $\sim$25 wt % olivine fractionation. The parental liquid of the gabbro GOR 508 has lower REE content than the komatiite liquid. This suggests that the calculated REE content is too low and that olivine is not the only phase to fractionate in this sample or that its liquid MgO content is overestimated. The dunites can be explained by $\sim$20 wt % olivine fractionation of the parental liquid of G2 komatiites.

This modelling strongly suggests that the intrusive and volcanic rocks on Gorgona Island are closely related and derived from a common parent. The parental magma of the intrusive rocks probably differentiated to basaltic compositions in magma chambers deeper in the crust whereas the komatiites and picrites bypassed these chambers and erupted directly as ultramafic liquids.

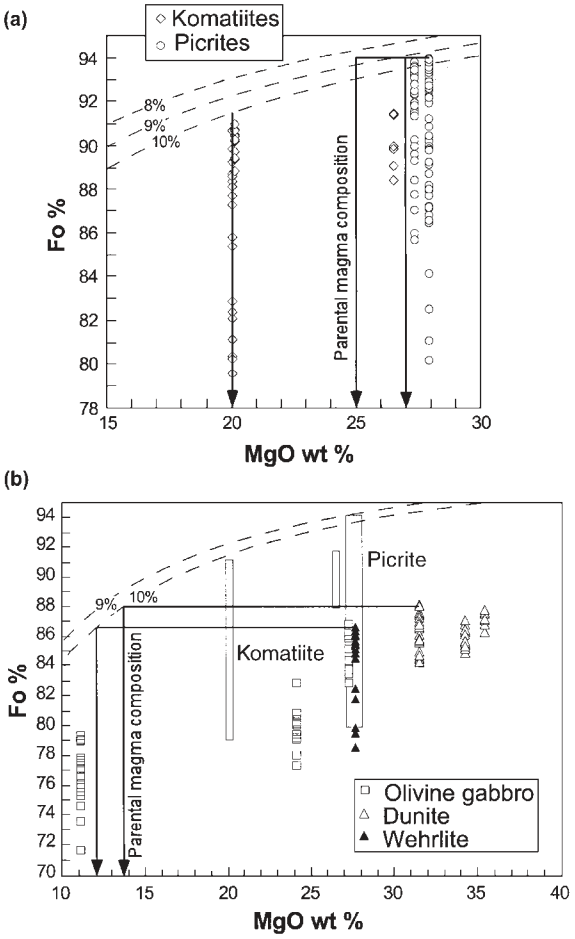

Fig. 8. MgO of whole rocks vs Fo contents of olivine from (a) komatiites and picrites, and (b) gabbros, dunites and wehrlites. The curves represent the liquid MgO content calculated from the Fo content of olivine in equilibrium with liquids containing 8, 9 and 10 wt % FeO. The calculations were made using an Mg–Fe olivine–liquid partition coefficient of 0·3 (Roeder & Emslie, 1970). Boxes in (b) indicate the range of olivine composition in komatiites and picrites.

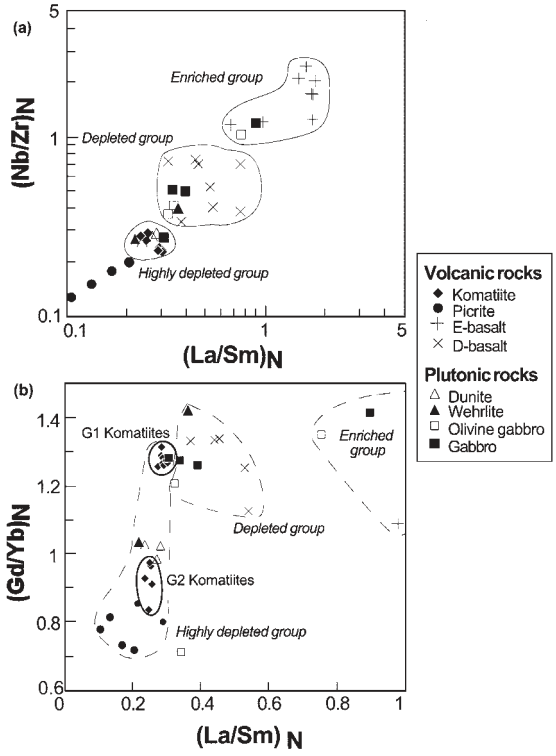

Fig. 9. (a) Nb/Zr vs La/Sm, normalized to the primitive mantle (Hofmann, 1988). The fields identify the three different trace element signatures referred to in the text. (b) La/Sm vs Gd/Yb, normalized to the primitive mantle (Hofmann, 1988). The fields G1 and G2 identify the two komatiite groups. In (a) and (b), source of data for E- and D-basalts as for Fig. 7.

Depth, degree and partial melting processes

Trace-element signatures in Gorgona plutonic and volcanic rocks vary widely, from almost flat REE patterns in gabbros and basalts, to extremely depleted patterns in the dunites and ultramafic lavas (Figs 6 and 9). It appears from the previous section that almost all rock types can be linked to high-MgO parental liquids, either directly or through olivine fractionation. Now we must explain the formation of high-MgO liquids showing a degree of depletion of incompatible trace element that greatly exceeds that of normal oceanic basalts.

Such unusual compositions can be related to either variable depletion in the source or processes that yielded incompatible-element-depleted liquids from a less depleted source. In other words, either the source of Gorgona rocks underwent a depletion event before it became part of the Gorgona plume, or the source became depleted during the partial melting that formed the Gorgona high-MgO liquids. Arndt *et al.* (1997) argued that source depletion well before the Gorgona event is unlikely because it should have resulted in large variations in Nd isotopic compositions and a positive correlation between Sm/Nd and the Nd isotope composition. The data plotted in Fig. 7 show that this is not the case. Arndt *et al.* (1997) suggested instead that the variable extents of incompatible-element depletion in the Gorgona lavas arose mainly through fractional melting in a common, moderately depleted source.

From their isotopic compositions, it can be inferred that the mantle source(s) of most Gorgona rocks became moderately depleted in incompatible element long before the Gorgona event. The long-term $^{147}Sm/^{144}Nd$ of this source can be calculated as 0·2, a value similar to that of normal depleted upper mantle and very different from the values of 0·26–0·46 recorded in Gorgona samples. In this section we explore the melting processes that can form highly depleted liquids from a less depleted source. Batch melting can be eliminated because it is able to explain neither the variability of

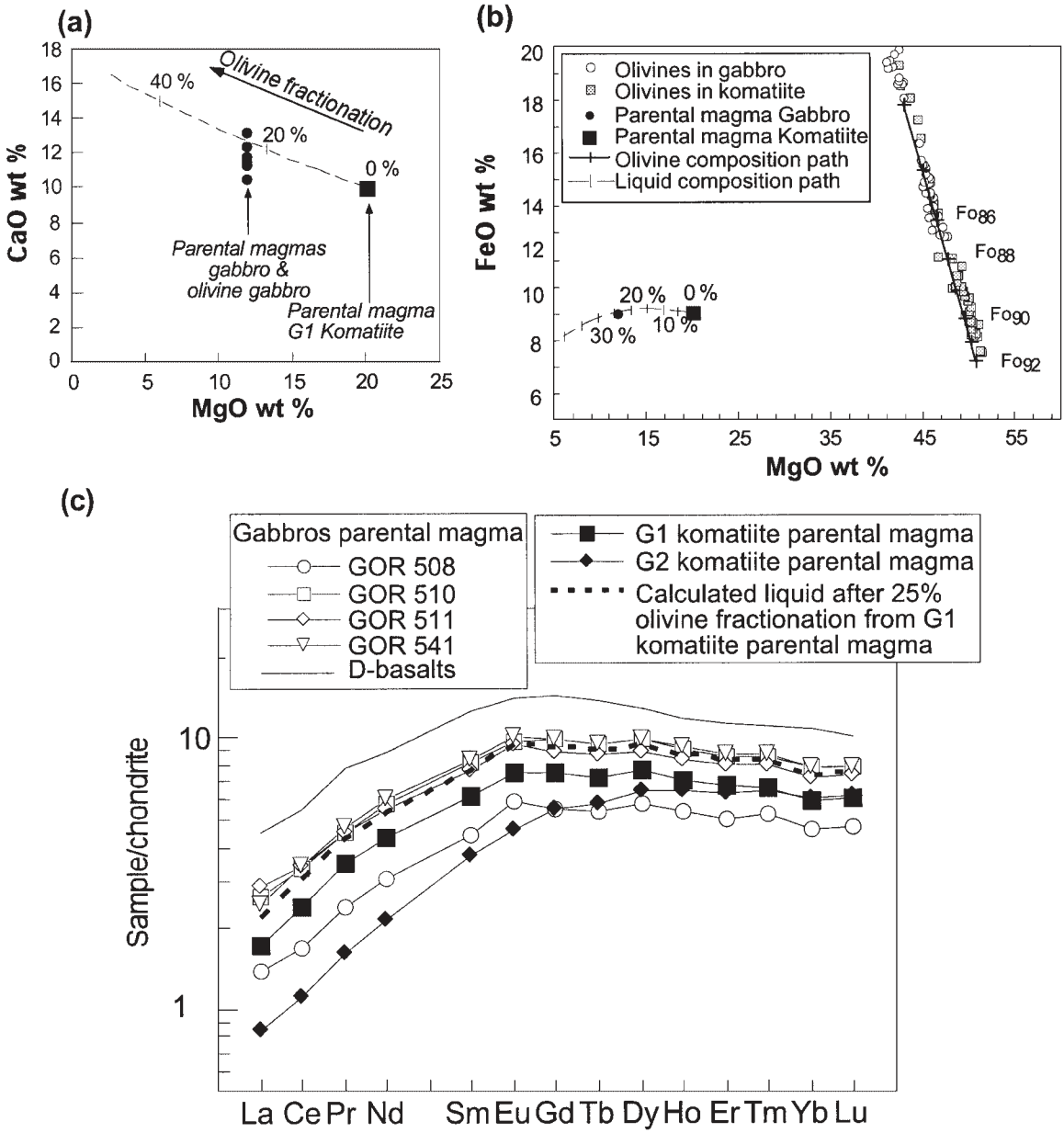

Fig. 10. (a) MgO (wt %) vs CaO (wt %) for the calculated parental magma compositions of G1 komatiites and gabbros. The dashed line represents the olivine fractionation path from G1 komatiites parental magma composition. Ticks show 20% and 40% increments. (b) MgO (wt %) vs FeO (wt %) for the calculated parental magma compositions of G1 komatiites and gabbros. The dashed line represents the liquid path produced by olivine fractionation from the G1 komatiite parental magma composition. Ticks show 5% increments. Also plotted are the olivine compositions for gabbros and komatiites. The bold line represents the olivine composition path from G1 komatiite parental magma. (c) Calculated REE patterns, normalized to chondrites (Sun & McDonough, 1989) for the parental magmas of G1 komatiites and gabbros. These were calculated by regressing their REE contents to the estimated MgO contents for the parental magmas (see text for details). The dotted line represents the calculated REE pattern after 25% olivine fractionation of G1 komatiite parental magma. Also shown for comparison are a typical REE pattern for D-basalt parental magma and G2 komatiite calculated parental magma.

REE patterns of Gorgona rocks nor the extent to which depletion exceeds that of normal mantle rocks. Given the high melting degree required to form high-MgO liquids, and taking into account experiments on peridotite melting, which show that melt can be extracted at degrees of melting as low as 1% [Sparks (1992) and references therein], we conclude that batch melting is unlikely. By contrast, fractional melting depletes the source through liquid extraction and leads to the formation of highly depleted liquids. Critical

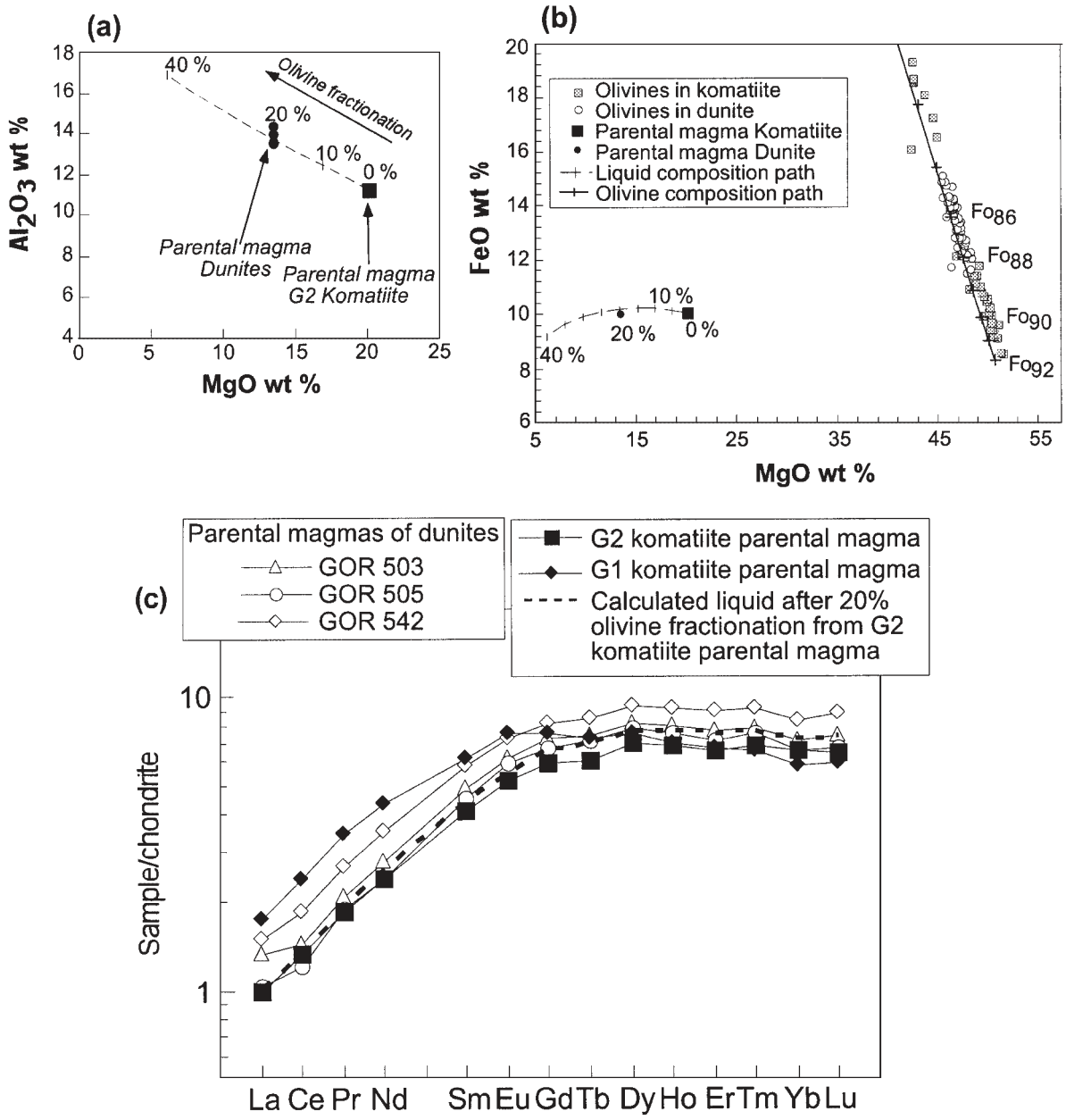

Fig. 11. (a) MgO (wt %) vs Al_2O_3 (wt %) for the calculated parental magma compositions of G2 komatiites and dunites. (b) MgO (wt %) vs FeO (wt %) for the calculated parental magma compositions of G2 komatiites and dunites. Also plotted are the olivine compositions for dunites and komatiites. (c) Calculated REE patterns for G2 komatiites and dunites parental magmas. (See caption of Fig. 10 for further details.)

melting, a variant of fractional melting in which a constant proportion of liquid remains in the source (Sobolev & Shimizu, 1993), was proposed by Arndt *et al.* (1997) to explain the formation of Gorgona rocks. Here we extend this model to explain the three main types of high-MgO liquids found on Gorgona—those parental to G1 komatiites, to G2 komatiites and to the picrites.

The main goal of the modelling was to reproduce the REE patterns of the three main types of high-MgO liquids. To simplify the procedure, we used the same source composition, a similar critical melting process, similar partition coefficients and similar melting modes. Two different mineral assemblages—garnet peridotite and spinel peridotite—were used to allow for the effects of decreasing pressure in a rising source. This entailed

Table 5: Parameters used in the partial melting modelling

Rock type:	G1 Komatiites	G2 Komatiites			Picrites		
		Step 1	Step 2	Total	Step 1	Step 2	Total
F:	14–16%	10%	4–8%	14–18%	10%	12–18%	22–28%
Source mineralogy (%)							
Ol	50	50	55		50	55	
Opx	15	10	15		10	15	
Cpx	25	30	25		30	25	
Spinel	0	0	5		0	5	
Gar	10	10	0		10	0	
Melting mode (%)							
Ol	3	3	10		3	10	
Opx	3	3	20		3	20	
Cpx	44	44	68		44	68	
Spinel	0	0	2		0	2	
Gar	50	50	0		50	0	
Source composition (× primitive mantle)							
La	0·50	0·50	0·05		0·50	0·05	
Ce	0·59	0·59	0·07		0·59	0·07	
Nd	0·72	0·72	0·19		0·72	0·19	
Sm	0·83	0·83	0·46		0·83	0·46	
Eu	0·89	0·89	0·59		0·89	0·59	
Dy	1·00	1·00	0·79		1·00	0·79	
Er	0·98	0·98	0·82		0·98	0·82	
Yb	1·03	1·03	0·91		1·03	0·91	
	Partition coefficients						
	Olivine	Opx	Cpx[1]	Cpx[2]	Spinel	Garnet	
La	$3{\cdot}1 \times 10^{-5}$	$4{\cdot}4 \times 10^{-5}$	$2{\cdot}9 \times 10^{-1}$	$5{\cdot}4 \times 10^{-2}$	$6{\cdot}0 \times 10^{-4}$	$1{\cdot}0 \times 10^{-3}$	
Ce	$1{\cdot}0 \times 10^{-4}$	$1{\cdot}4 \times 10^{-4}$	$3{\cdot}1 \times 10^{-1}$	$8{\cdot}6 \times 10^{-2}$	$6{\cdot}0 \times 10^{-4}$	$4{\cdot}0 \times 10^{-3}$	
Nd	$4{\cdot}2 \times 10^{-4}$	$5{\cdot}2 \times 10^{-4}$	$4{\cdot}0 \times 10^{-1}$	$1{\cdot}9 \times 10^{-1}$	$6{\cdot}0 \times 10^{-4}$	$5{\cdot}7 \times 10^{-2}$	
Sm	$1{\cdot}1 \times 10^{-3}$	$1{\cdot}6 \times 10^{-3}$	$5{\cdot}9 \times 10^{-1}$	$2{\cdot}9 \times 10^{-1}$	$6{\cdot}0 \times 10^{-4}$	$6{\cdot}3 \times 10^{-1}$	
Eu	$8{\cdot}0 \times 10^{-4}$	$6{\cdot}4 \times 10^{-4}$	$5{\cdot}9 \times 10^{-1}$	$3{\cdot}5 \times 10^{-1}$	$6{\cdot}0 \times 10^{-4}$	1	
Dy	$1{\cdot}4 \times 10^{-3}$	$8{\cdot}4 \times 10^{-3}$	$7{\cdot}8 \times 10^{-1}$	$4{\cdot}4 \times 10^{-1}$	$1{\cdot}5 \times 10^{-3}$	2	
Er	$1{\cdot}3 \times 10^{-2}$	$1{\cdot}7 \times 10^{-2}$	$8{\cdot}2 \times 10^{-1}$	$3{\cdot}9 \times 10^{-1}$	$3{\cdot}0 \times 10^{-3}$	3	
Yb	$3{\cdot}0 \times 10^{-2}$	$3{\cdot}3 \times 10^{-2}$	$8{\cdot}0 \times 10^{-1}$	$4{\cdot}3 \times 10^{-1}$	$4{\cdot}5 \times 10^{-3}$	4	

Source compositions were calculated after the value of Gurenko & Chaussidon (1995) and resemble the depleted mantle. Melting modes from Johnson (1990). Partition coeficients are from Gurenko & Chaussidon (1995). Two sets of partition coefficients were used for clinopyroxenes; Cpx[1] were used for high pressures (garnet field) and are from Shimizu (1982). Cpx[2] are used for lower pressures (spinel field) and are from Gurenko & Chaussidon (1995).

the use of two different clinopyroxene partition coefficients, and two sets of melting modes (Table 5). The source composition was inferred, on the basis of Nd isotopic compositions, to be depleted in incompatible elements. We chose to use data from Gurenko & Chaussidon (1995) for moderately depleted upper-mantle peridotite. The results are shown in Fig. 12 and the parameters used in the modelling are listed in Table 5.

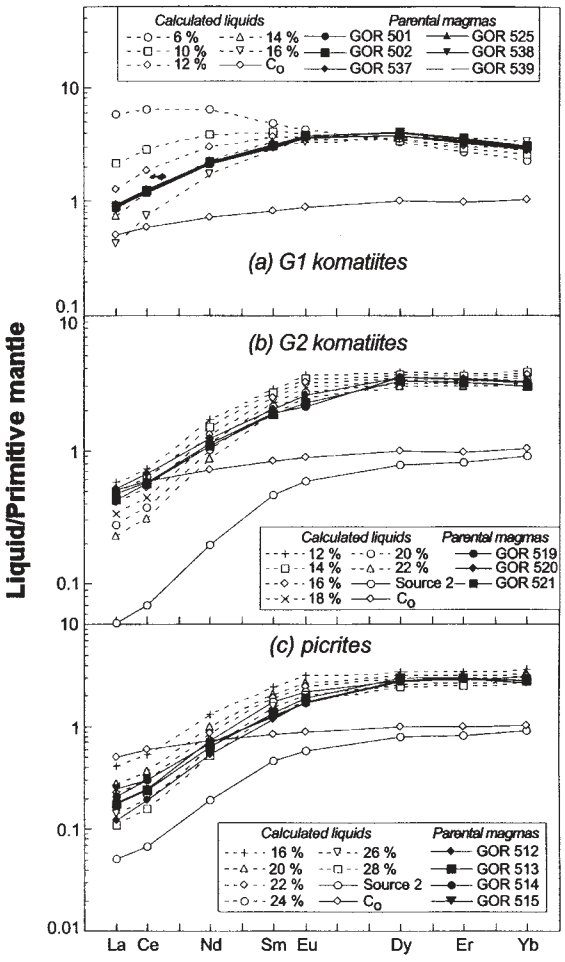

Fig. 12. Calculated REE patterns (filled symbols), normalized to the primitive mantle (Hofmann, 1988), for parental magmas of (a) G1 komatiites, (b) G2 komatiites and (c) picrites. In each diagram, dashed lines correspond to calculated liquid compositions resulting from different degrees of critical melting. C_0 pattern is the source composition used in the modelling (see also text and Table 5). In (b) and (c) 'Source 2' is the intermediate source composition calculated for two-stage partial melting (see also text and Table 5).

G1 komatiites

G1 komatiites are depleted both in LREE and HREE (Fig. 12a), a pattern we interpret to indicate that melting started deep in the mantle, in the field of garnet stability. Such REE patterns can be reproduced by 14–16% critical melting with the retention of 3% liquid in the residue. The HREE depletion is due to the persistence of garnet throughout the melting interval; the LREE depletion results from continued extraction of partial melt, which accentuates the initial slight depletion of the source.

G2 komatiites

G2 komatiites are slightly more depleted in LREE but have flat HREE patterns. The difference in HREE patterns between G1 and G2 komatiites can be explained in three different ways: (1) a higher degree of partial melting, with the result that all garnet was consumed before the segregation of G2 komatiites; (2) melting at shallower depths in the mantle and entirely within the spinel stability field; or (3) melting that started within the garnet stability field but continued in the spinel stability field as a result of continuing ascent of the mantle source.

The first hypothesis can be rejected on the basis that there do not seem to be any differences between the two groups of komatiite in overall concentrations of REE, nor in the MgO contents of the parental magmas, as estimated from olivine compositions. Such differences would be expected if the percentage of melting were very different. In the case of melting entirely within the spinel stability field, the general shape of the REE pattern is reproduced but the extent of depletion of LREE is far too high and HREE concentrations are too high.

Our preferred model is presented in Fig. 12b and listed in Table 5. We assumed critical melting with 3% residual liquid and 15% total partial melting, but modelled melting in two stages, with 10% in the garnet stability field (referred to as 'Step 1' in Table 5) followed by ~5% in the spinel field (referred to as 'Step 2' in Table 5). To model this process, we recalculated the source composition at the start of the second stage using mass balance between the calculated composition of the residue of the previous stage and the original source composition. These two source compositions are identified as 'source composition' of Step 1 and 2 in Table 5 and as C_0 and 'Source 2' in Fig. 12b. The REE patterns of G2 komatiites are reproduced using this approach but the source mineralogy during the second stage is peculiar, having a higher proportion of clinopyroxene than is usually proposed for the mantle. A melting model with the same two stages, but with a more normal clinopyroxene-poor mineralogy leads to a liquid that has the same shape as G2 komatiites, but with higher concentrations for both LREE and HREE. The compositions of G2 komatiites are slightly less well reproduced than those of G1 komatiites, in that the LREE depletion of the calculated liquids is slightly too high and the curvature of the pattern is too pronounced. However, given the uncertainties of two-stage melting calculations, the agreement between the calculated liquids and G2 komatiites seems reasonable.

To summarize, we consider that all komatiitic liquids are produced by a similar melting process, with similar degrees of melting. For both types of komatiite, melting started in the garnet field, but for the G2 komatiites melting continued into the spinel field. This difference may be related to differences in source temperature. A source with relatively low temperature, if rising along an adiabatic melting path, will reach the solidus at relatively low pressure and could pass from the garnet to spinel

field while the degree of melting was relatively low. For a source at higher temperature, which would intersect the mantle solidus at greater depths (McKenzie & Bickle, 1988), all the melting may take place in the garnet field. Such a difference in temperature would not, however, lead to large differences in the major-element composition of the liquids (Herzberg, 1992). A second important aspect of the modelling is the high clinopyroxene content of the source particularly for the G2 komatiites. This could reflect the presence in the source of recycled pyroxene-rich cumulates from oceanic crust as proposed by Lassiter & Hauri (1998) and Chauvel & Hémond (2000) for oceanic island basalts.

Picrites

The parental liquid for the picrites was modelled in the same manner as for the komatiites (Fig. 12c, Table 5). These rocks are extremely depleted in LREE with flat to slightly depleted HREE patterns. As for G2 komatiites, these patterns are best reproduced by melting that started in the garnet stability field and finished in the spinel field. As expected from the high MgO content of the parental liquid (25 $\pm$ 2 wt %) and the lower concentrations of REE, the degree of melting was higher than for komatiites, at $\sim$25%, with 10% in the garnet field followed by 12–16% in the spinel field (Table 5 and Fig. 12c). As proposed for the G2 komatiites, the source must be particularly rich in clinopyroxene (25 wt %), to explain the low concentrations in both LREE and HREE. Thus, although the picrites and the G2 komatiites were produced from a source with the same initial composition, the more advanced melting for the picrites led to the extreme depletion in incompatible elements that characterizes these rocks.

Modelling major elements

To confirm the results of the REE modelling, we modelled the major-element compositions of the parental liquids of the komatiites and picrites. To calculate the compositions of liquids formed through critical melting, we used the high-pressure partition coefficients for major elements obtained by Herzberg & Zhang (1996) during experiments on the peridotite KBL-1. The source composition was that of the same peridotite and a pressure of 5 GPa was adopted, following Herzberg (1992) and Nisbet *et al.* (1993). The procedure used was as follows: (1) using the partition coefficients, we calculated the composition of a liquid in equilibrium with the original source for the first small (1%) increment of melting; (2) using mass balance between the calculated liquid and the original source, a new source composition was calculated; (3) from this composition and the same partition coefficients, a second liquid was calculated. Up to 25 iterations were made, corresponding to 25% cumulative melting, the degree inferred for picrites from REE modelling. The results are presented in Fig. 13.

Given the uncertainties of both the calculations and the experimental partition coefficients, the agreement with the calculated parental liquid compositions shown in Fig. 13 is reasonable. It should be noted, however, that the MgO content at 25% cumulative melting is lower than that of the picritic parental liquid. This can be explained in several ways; for example: (1) the source may have been more refractory than that used in the modelling; or (2) the pressure at which the picritic liquid formed was slightly higher, resulting in a larger MgO content of the liquids.

Intrusive rocks

Two olivine gabbros (GOR 534 and GOR 535) have almost flat REE patterns (Figs 6 and 9) and their general trace-element characteristics are close to those of the E-basalts (Kerr *et al.*, 1996). Moreover, their isotopic compositions are relatively enriched, again like those of the E-basalts (Fig. 7). This indicates that these two rock types are petrogenetically related to these basalts and did not form from the same mantle source as the komatiites. The derivation of magmas with flat REE patterns from a depleted mantle source, a general feature of oceanic plateau basalts, can be interpreted in terms of pooling of liquids formed by fractional melting at different depths and homogenized en route to the surface (Kerr *et al.*, 1997*b*; Révillon *et al.*, 1999, 2000). The E-basalts, which are slightly enriched in LREE and depleted in HREE (Kerr *et al.*, 1996; Arndt *et al.*, 1997) could be representative of a separate stage of liquid extraction. The primary liquids formed at great depth and relatively low degrees of melting, as indicated by their HREE depletion and high incompatible element concentrations. The E-basalts erupted as lava flows, but the liquids that formed the olivine gabbros were trapped and crystallized in magma chambers.

Mantle sources

The Nd isotopic data allow us to distinguish two different mantle sources involved in the petrogenesis of the magmas (Fig. 7). The first, well-sampled, source is isotopically depleted, with initial ε_{Nd} ranging from $+10{\cdot}4$ to $+8{\cdot}2$. It produced the komatiites, picrites, gabbros, dunites and wehrlites. The second, less depleted and more rarely sampled source had compositions ranging from ε_{Nd} $+5{\cdot}3$ to $+7{\cdot}6$. It yielded the E-basalts (Kerr *et al.*, 1996; Arndt *et al.*, 1997), some of the gabbros, a dunite and a picrite. In view of the close spatial and temporal relationship between these magmas, it is evident that the plume source of the Gorgona magmas was originally isotopically heterogeneous at a small scale. The large range in $^{147}Sm/$

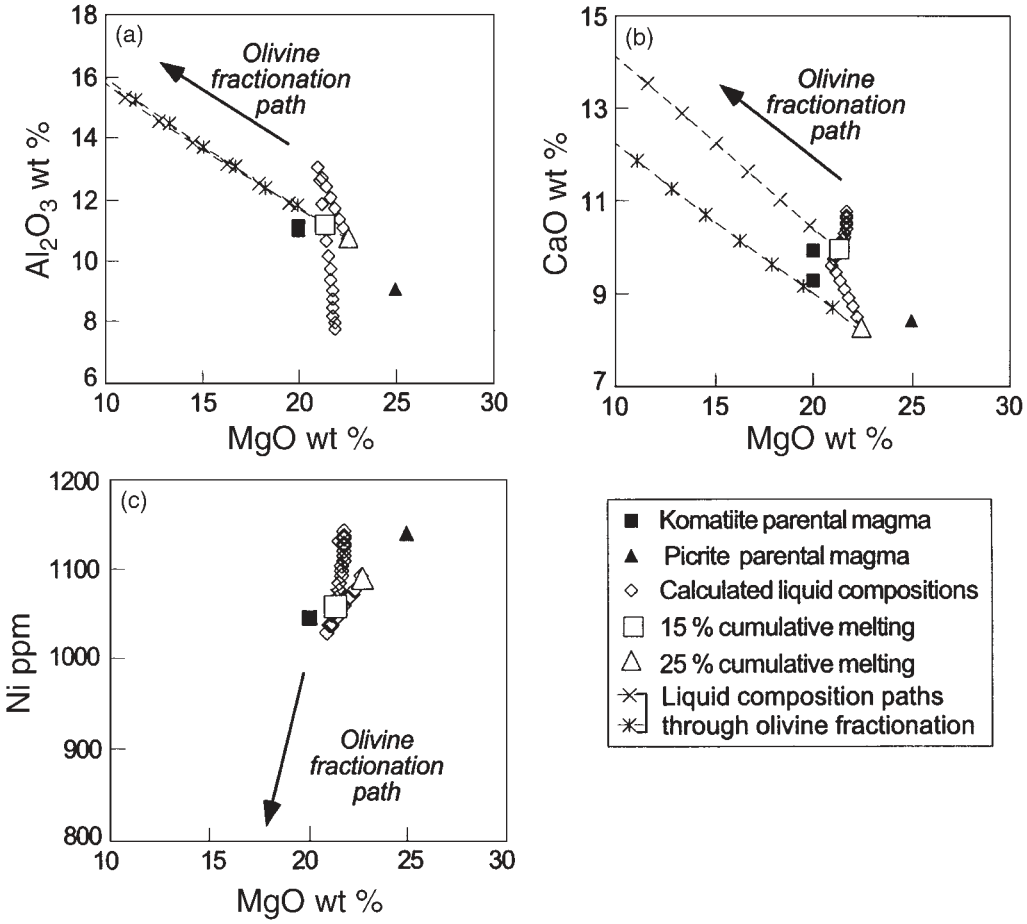

Fig. 13. MgO (wt %) vs Al_2O_3 (wt %), CaO (wt %) and Ni (ppm) of liquids produced through fractional melting at 5 GPa (◇) and the parental magmas for komatiites (■) and picrites (▲). □, △, liquids compositions produced by 15% and 25% melting, respectively. Dashed lines represent olivine fractionation paths from the latter two liquids. Crosses represent 5% olivine fractionation.

^{144}Nd ratios, on the other hand, finds a ready explanation in the partial melting process.

CONCLUSIONS

Plumbing system of an oceanic plateau

The volcanic and intrusive rocks of Gorgona were derived from magmas with a wide range of compositions; komatiites and picrites crystallized directly from liquids with 20 $\pm$ 2 to 25 $\pm$ 2 wt % MgO whereas the gabbros, wehrlites and dunites formed through the accumulation of olivine and pyroxene from liquids with basaltic compositions (MgO $\leq$ 13 wt %). Similarities in the trace-element characteristics of the majority of intrusive rocks and the ultramafic lavas indicate that they had similar or common parental magmas. It appears that the basaltic liquids from which the intrusive rocks were derived resulted from variable amounts of mainly olivine fractionation from parental ultramafic magmas. Textures indicative of rapid cooling suggest that the intrusive rocks were emplaced at a high level within the volcanic pile.

These observations and inferences provide the basis of the multi-stage model for the plumbing system of the Gorgona plateau illustrated in Fig. 14. The ultramafic magmas, parental to the intrusive rocks of Gorgona, differentiated to basaltic compositions before these magmas were emplaced at their present level in the volcanic pile. The products of this differentiation were (1) basaltic liquids, which ascended towards the surface where they were emplaced as sills or erupted as lavas, and (2) a thick layer of ultramafic cumulates. This differentiation took place at a deeper level, perhaps in magma chambers located at or near the base of the crust. The presence of such a layer may explain the presence of high-velocity, high-density material identified in geophysical surveys elsewhere in the Caribbean plateau (Case *et al.*, 1990; Leroy & Mauffret, 1996; Mauffret & Leroy, 1997). Not all the ultramafic magma was processed in the

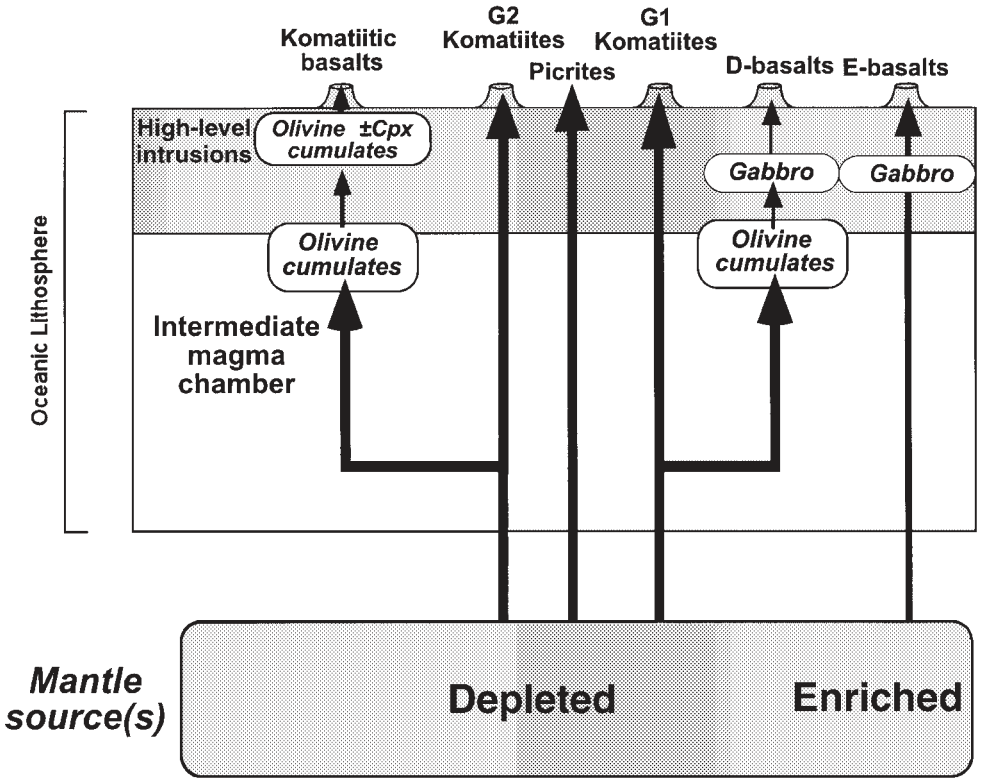

Fig. 14. Multi-stage model for the plumbing system of the Gorgona plateau. G1 and G2 komatiites and picrites are extracted from a mantle source that had been depleted in incompatible elements through advanced fractional melting. Some of these liquids were trapped in magma chambers where they differentiated to give gabbros and olivine–clinopyroxene cumulates (dunites and wehrlites). The two gabbros with flat REE patterns are linked to the E-basalts. They form through pooling of liquids from a different mantle source. The D-basalts are the volcanic equivalent of the gabbros. The extrusive equivalent of olivine cumulates was not directly identified but could be represented by the less MgO-rich G2 komatiite GOR 520 (komatiitic basalt).

chamber and some of it passed directly to the surface to erupt as komatiitic and picritic volcanic rocks.

Plume composition and melting processes

The Nd isotopic compositions indicate that the mantle source of Gorgona rocks was heterogeneous. One component, which had highly depleted isotopic compositions, yielded the ultramafic magmas parental to the komatiites, picrites and intrusive ultramafic rocks. The second, less depleted component was the dominant source of the E-basalts and certain gabbros. The large range in trace-element ratios in Gorgona lavas resulted from critical melting that led to progressive depletion of the more incompatible elements in the source of the ultramagnesian magmas.

ACKNOWLEDGEMENTS

The authors are grateful to Gustavo Garzon (Ministerio del Medio Ambiante, Cali, Colombia) for his assistance in arranging permission to visit Gorgona, and to Claudia Isabel Acevedo and Gustavo Mayor for help and logistic support in the field. We are grateful to A. C. Kerr for providing some of his Gorgona samples and analysis. We also thank Nicole Morin and Joèl Macé for their assistance with the isotopic analyses in Rennes; Martine Lecoz-Bounhik for help with XRF analyses in Rennes; Liliane Savoyan for help in ICP-MS analyses at the University of Montpellier; Marcel Bohn, in Brest, and Rob Wilson, in Leicester, for their assistance with microprobe analyses. This manuscript was improved through discussions with Ramon Capdevila and Bor Ming Jahn, and reviews by Dennis Geist, Cinzia Farnetani, Mike Cheadle and Marjorie Wilson. This work was supported by the French CNRS (grants in the IDYL and IT programme to N.T.A.).

REFERENCES

Aitken, B. G. & Echeverria, L. M. (1984). Petrology and geochemistry of komatiites and tholeiites from Gorgona Island, Colombia. *Contributions to Mineralogy and Petrology* **86**, 94–105.

Arndt, N. T. (1986). Differentiation of komatiite flows. *Journal of Petrology* **27**, 279–301.

Arndt, N. T., Kerr, A. C. & Tarney, J. (1997). Dynamic melting in plume heads: the formation of Gorgona komatiites and basalts. *Earth and Planetary Science Letters* **146**, 289–301.

Bickle, M. J. (1982). The magnesium contents of komatiitic liquids. In: Arndt, N. T. & Nisbet, E. G. (eds) *Komatiites*. London: George Allen and Unwin, pp. 479–494.

Burke, K. (1988). Tectonic evolution of the Caribbean. *Annual Review of Earth and Planetary Sciences* **16**, 201–230.

Case, J. E., Macdonald, W. D. & Fox, P. J. (1990). Caribbean crustal provinces; seismic and gravity evidence. In: Dengo, G. & Case, J. E. (eds) *The Caribbean Region. The Geology of North America*. Boulder, CO: Geological Society of America, pp. 15–36.

Chauvel, C. & Hémond, C. (2000). Melting of a complete section of recycled oceanic crust: trace element and Pb isotopic evidence in Iceland. *Geochemistry, Geophysics and Geosystems* **1**.

Cloos, M. (1993). Lithospheric buoyancy and collisional orogenesis: subduction of oceanic plateaux, continental margins, island arcs, spreading ridges and seamounts. *Geological Society of America Bulletin* **105**, 715–737.

Coffin, M. F. & Eldholm, O. (1993). Scratching the surface: estimating dimensions of large igneous provinces. *Geology* **21**, 515–518.

Coffin, M. F. & Eldholm, O. (1994). Large igneous provinces: crustal structure, dimensions, and external consequences. *Reviews of Geophysics* **32**, 1–36.

Cohen, R. S. & O'Nions, R. K. (1982). The lead, neodymium and strontium isotopic structure of ocean ridge basalts. *Journal of Petrology* **23**, 299–324.

Cox, K. G. (1980). A model for flood basalt vulcanism. *Journal of Petrology* **21**, 629–650.

Donaldson, C. H. (1979). An experimental investigation of the delay in nucleation of olivine in mafic lavas. *Contributions to Mineralogy and Petrology* **69**, 21–32.

Duncan, R. A. & Hargraves, R. B. (1984). Plate tectonic evolution of the Caribbean region in the mantle reference frame. In: Bonini, W. E., Hargraves, R. B. & Shagam, R. (eds) *The Caribbean–South American Plate Boundary and Regional Tectonics. Geological Society of America, Memoir* **162**, 81–84.

Echeverria, L. M. (1980). Tertiary or Mesozoic komatiites from Gorgona Island, Colombia: field relations and geochemistry. *Contributions to Mineralogy and Petrology* **73**, 253–266.

Echeverria, L. M. (1982). Komatiites from Gorgona island, Colombia. In: Arndt, N. T. & Nisbet, E. G. (eds) *Komatiites*. London: George Allen and Unwin, 526 pp.

Echeverria, L. M. & Aitken, B. G. (1986). Pyroclastic rocks: another manifestation of ultramafic volcanism on Gorgona Island, Colombia. *Contributions to Mineralogy and Petrology* **92**, 428–436.

Farnetani, C. G., Richard, M. A. & Ghiorso, M. S. (1996). Petrological models of magma evolution and deep crustal structure beneath hotspots and flood basalt provinces. *Earth and Planetary Science Letters* **143**, 81–94.

Francis, P. (1993). *Volcanoes: a Planetary Perspective*. Oxford: Oxford University Press, 443 pp.

Gansser, A. (1950). Geological and petrological notes on Gorgona island in relation to North-West S. America. *Schweizerische Mineralogische und Petrographische Mitteilungen* **30**, 219–237.

Gansser, A., Dietrich, V. J. & Cameron, W. E. (1979). Paleogene komatiites from Gorgona island. *Nature* **278**, 545–546.

Gurenko, A. A. & Chaussidon, M. (1995). Enriched and depleted primitive melts included in olivine from Icelandic tholeiites: origin by continuous melting of a single mantle column. *Geochimica et Cosmochimica Acta* **59**, 2905–2917.

Hauff, F. K., Hoernle, H., Schminke, U. & Werner, R. A. (1997). Mid-Cretaceous origin for the Galapagos hotspot: volcanological, petrological and geochemical evidence from Costa Rican oceanic crustal fragments. *Geologishe Rundschau* **86**, 141–155.

Hauff, F., Hoernle, K., Tilton, G., Graham, D. W. & Kerr, A. C., (2000). Large volume recycling of oceanic lithosphere over short time scale: geochemical constraints from the Caribbean Large Igneous Province. *Earth and Planetary Science Letters* **174**, 247–263.

Herzberg, C. (1992). Depth and degree of melting of komatiites. *Journal of Geophysical Research* **97**, 4521–4540.

Herzberg, C. & Zhang, J. (1996). Melting experiments on anhydrous peridotite KLB-1: composition of magmas in the upper mantle and transition zone. *Journal of Geophysical Research* **101**, 8271–8295.

Hill, R. E. T., Gole, M. J. & Barnes, S. J. (1989). Olivine adcumulates in the Norseman–Wiluna greenstone belt, Western Australia: implications for the volcanology of komatiites. In: Prendergast, M. D. & Jones, M. J. (eds) *Magmatic Sulphides—The Zimbabwe Volume*, pp. 189–206.

Hofmann, A. W. (1988). Chemical differentiation of the Earth: the relationship between mantle, continental crust, and oceanic crust. *Earth and Planetary Science Letters* **90**, 297–314.

Johnson, K. T., Dick, H. J. B. & Shimizu, N. (1990). Melting in the oceanic upper mantle: an ion microprobe study of diopsides in abyssal peridotites. *Journal of Geophysical Research* **95**, 2661–2678.

Kerr, A. C., Marriner, G. F., Arndt, N. T., Tarney, J., Nivia, A., Saunders, A. D. & Duncan, R. (1996). The petrogenesis of Gorgona komatiites, picrites and basalts: new field, petrographic and geochemical constraints. *Lithos* **37**, 245–260.

Kerr, A. C., Marriner, G. F., Tarney, J., Nivia, A., Saunders, A. D., Thirlwall, M. F. & Sinton, C. W. (1997*a*). Cretaceous basaltic terranes in Western Colombia: elemental, chronological and Sr–Nd isotopic constraints on petrogenesis. *Journal of Petrology* **38**, 677–702.

Kerr, A. C., Tarney, J., Marriner, G., Nivia, A. & Saunders, A. D. (1997*b*). The Caribbean–Colombian Cretaceous Igneous Province: the internal anatomy of an oceanic plateau. In: Mahoney, J. J. & Coffin, M. F. (eds) *Large Igneous Provinces: Continental, Oceanic and Planetary Flood Volcanism*. Washington, DC: American Geophysical Union, pp. 123–144.

Kerr, A. C., Tarney, J., Nivia, A., Marriner, G. F. & Saunders, A. D. (1998). The internal structure of oceanic plateau: inferences from obducted Cretaceous terranes in western Colombia and the Caribbean. *Tectonophysics* **292**, 173–188.

Lahaye, Y., 1995. L'altération des komatiites. Ph.D. Thesis, University of Rennes 1, 215 pp.

Lapierre, H., Bosch, D., Dupuis, V., Polvé, M., Maury, R. C., Hernandez, J., Monié, P., Yeghicheyan, D., Jaillard, E., Tardy, M., Mercier de Lépinay, B., Mamberti, M., Desmet, A., Keller, F. & Sénebier, F. (2000). Multiple plume events in the genesis of the peri-Caribbean Cretaceous oceanic plateau province. *Journal of Geophysical Research* (in press).

Lassiter, J. C. & Hauri, E. H. (1998). Osmium-isotope in Hawaiian lavas: evidence for recycled oceanic lithosphere in the Hawaiian plume. *Earth and Planetary Science Letters* **164**, 483–496.

Leroy, S., 1995. Structure et origine de la plaque Caraïbe. Implications géodynamiques. Ph.D. Thesis, University of Paris 6, 250 pp.

Leroy, S. & Mauffret, A. (1996). Intraplate deformation in the Caribbean region. *Journal of Geodynamics* **21**, 113–122.

Mahoney, J. J., Storey, M., Duncan, R. A., Spencer, K. J. & Pringle, M. (1993). Geochemistry and geochronology of Leg 130 basement lavas: nature and origin of the Ontong Java Plateau. In: Berger, W. H., Kroenke, L. W. & Mayer, L. A. (eds) *Proceedings of the Ocean Drilling Program, Scientific Results 130*. College Station, TX: Ocean Drilling Program, pp. 3–22.

Mauffret, A. & Leroy, S. (1997). Seismic stratigraphy and structure of the Caribbean igneous province. *Tectonophysics* **283**, 61–104.

McKenzie, D. P. & Bickle, M. J. (1988). The volume and composition of melt generated by extension of the lithosphere. *Journal of Petrology* **29**, 625–679.

Neal, C. R., Mahoney, J. J., Kroenke, L. W., Duncan, R. A. & Petterson, M. G. (1997). The Ontong Java Plateau. In: Mahoney, J. J. & Coffin, M. F. (eds) *Large Igneous Provinces: Continental, Oceanic and Planetary Flood Volcanism*. Washington, DC: American Geophysical Union, pp. 183–216.

Nesbitt, R. W. (1971). Skeletal crystal forms in the ultramafic rocks of the Yilgarn Block, Western Australia: evidence for an Archean ultramafic liquid. *Geological Society of Australia* **3**, 331–347.

Nisbet, E. G., Cheadle, M. J., Arndt, N. T. & Bickle, M. J. (1993). Constraining the potential temperature of the Archaean mantle: a review of the evidence from komatiites. *Lithos* **30**, 291–307.

Nivia, A. (1996). Evidence for obduction in the Bolivar ultramafic complex, SW Colombia. *Journal of South American Earth Science* **9**, 59–68.

Pindell, J. L. & Barrett, S. F. (1990). Geological evolution of the Caribbean region; a plate tectonic perspective. In: Dengo, G. & Case, J. E. (eds) *The Caribbean Region. The Geology of North America*. Boulder, CO: Geological Society of America, pp. 405–432.

Pindell, J. L., Cande, S. C., Pitman, W. C., III, Rowley, D. B., Dewey, J. F., LaBrecque, J. & Haxby, W. (1988). A plate-kinematic framework for models of Caribbean evolution. *Tectonophysics* **155**, 121–138.

Renner, R., Nisbet, E. G., Cheadle, M. J., Arndt, N. T., Bickle, M. J. & Cameron, W. E. (1993). Komatiite flows from the Reliance Formation, Belingwe Belt, Zimbabwe: I—petrography and mineralogy. *Journal of Petrology* **35**, 361–400.

Révillon, S., Arndt, N. T., Hallot, E., Kerr, A. C. & Tarney, J. (1999). Petrogenesis of picrites from the Caribbean plateau and the North Atlantic magmatic province. *Lithos* **49**, 1–21.

Révillon, S., Hallot, E., Arndt, N. T., Chauvel, C. & Duncan, R. A. (2000). A complex history for the Caribbean plateau: petrology, geochemistry and geochronology of the Beata ridge, south Hispaniola. *Journal of Geology* (in press).

Roeder, P. L. & Emslie, R. F. (1970). Olivine–liquid equilibrium. *Contributions to Mineralogy and Petrology* **29**, 275–289.

Saunders, A. D., Tarney, J., Kerr, A. C. & Kent, R. W. (1996). The formation and fate of large igneous provinces. *Lithos* **37**, 81–95.

Sinton, C. W., Duncan, R. A., Storey, M., Lewis, J. & Estrada, J. J. (1998). An oceanic flood basalt province within the Caribbean plate. *Earth and Planetary Science Letters* **155**, 221–235.

Smith, T. L. & Batiza, R. (1989). New field and laboratory evidence for the origin of hyaloclastite flows on seamount summits. *Bulletin of Volcanology* **51**, 96–114.

Sobolev, A. V. & Shimizu, N. (1993). Ultra-depleted primary melt included in an olivine from the Mid-Atlantic Ridge. *Nature* **363**, 151–154.

Sparks, S. J., 1992. Magma generation in the Earth. In: Brown, G., Hawkesworth, C. & Wilson, C. (eds) *Understanding the Earth*. Cambridge: Cambridge University Press, pp. 91–114.

Sun, S.-S. & McDonough, W. F. (1989). Chemical and isotopic systematics of oceanic basalts: implications for mantle composition and processes. In: Saunders, A. D. & Norry, M. J. (eds) *Magmatism in the Ocean Basins. Geological Society, London, Special Publication* **42**, 313–345.

White, W. M., Hofmann, A. W. & Puchelt, H. (1987). Isotope geochemistry of Pacific mid-ocean ridge basalts. *Journal of Geophysical Research* **92**, 4881–4893.

White, W. M., McBirney, A. R. & Duncan, R. A. (1993). Petrology and geochemistry of the Galápagos Islands: portrait of a pathological mantle plume. *Journal of Geophysical Research* **98**, 19533–19563.